AD-A078 484 CALIFORNIA STATE UNIV LONG BEACH DEPT OF MECHANICAL --ETC F/G 20/4
THE CALCULATION OF MOMENTUM AND HEAT TRANSFER IN INTERNAL FLOWS--ETC(U)
DEC 78 T CEBECI N00014-77-C-0073
UNCLASSIFIED ONR-CR297-002-1 NL

| OF |
AD
A078484

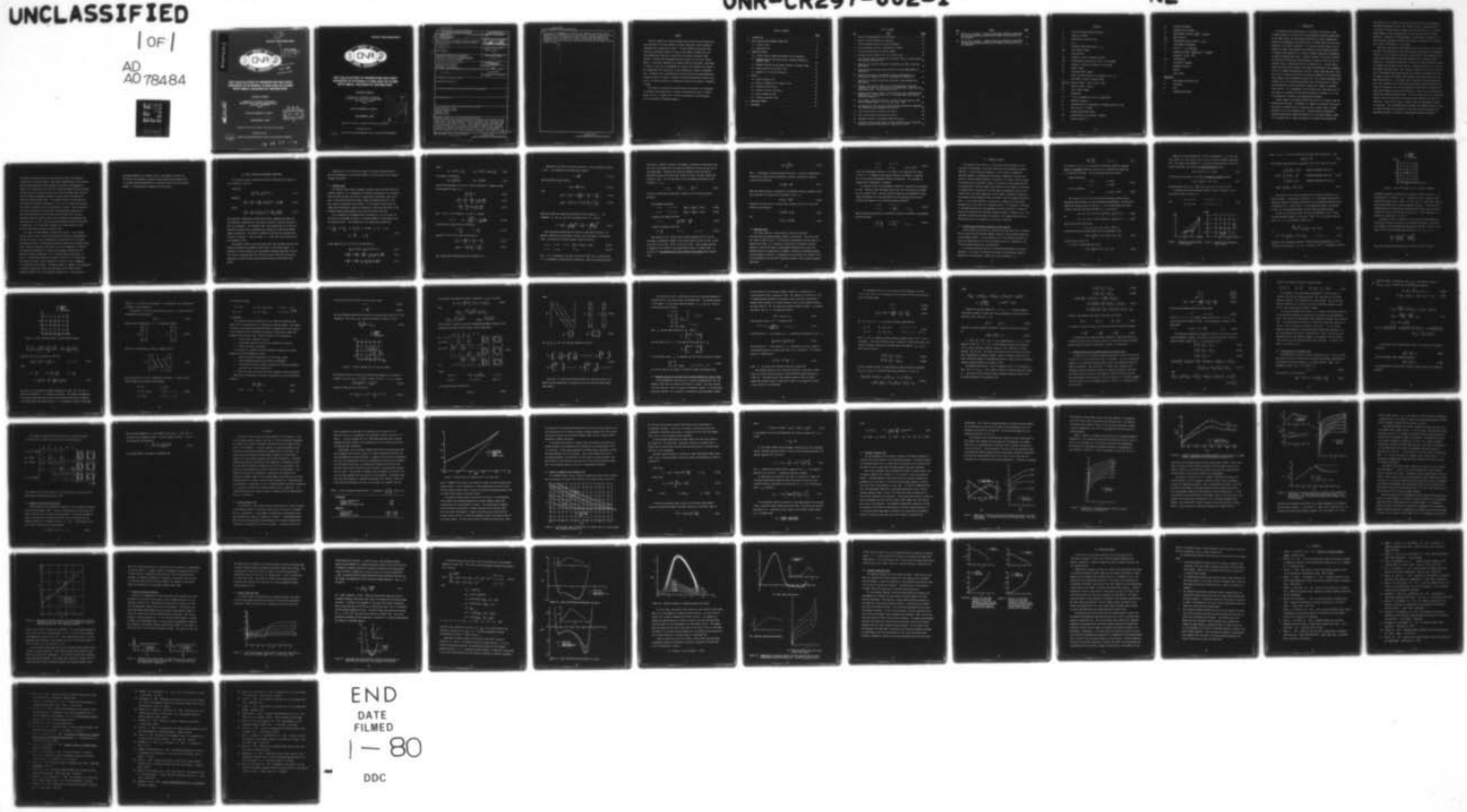

END
DATE
FILMED
1-80
DDC

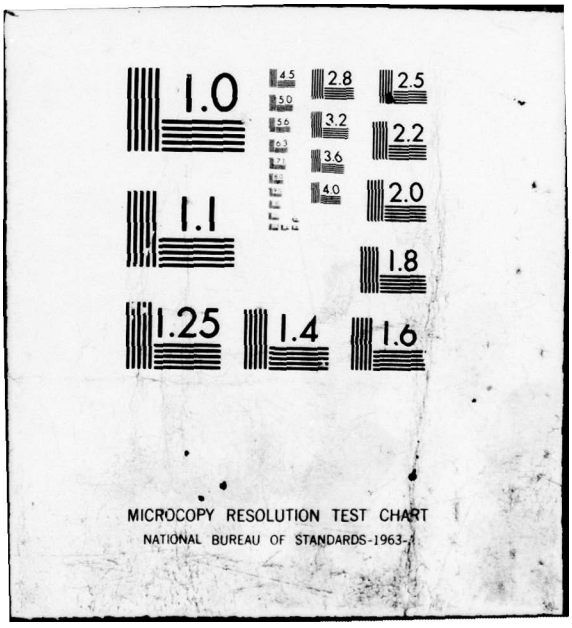
1.0
1.1
1.25
1.4
1.6
1.8
2.0
2.2
2.5
2.8
3.2
3.6
4.0
4.5
5.0
5.6
6.3
MICROCOPY RESOLUTION TEST CHART
NATIONAL BUREAU OF STANDARDS-1963-A

REPORT ONR-CR297-002-1

LEVEL II

THE CALCULATION OF MOMENTUM AND HEAT TRANSFER IN INTERNAL FLOWS AND IN FLOWS WITH SMALL REGIONS OF SEPARATION

TUNCER CEBECI

DEPARTMENT OF MECHANICAL ENGINEERING
CALIFORNIA STATE UNIVERSITY AT LONG BEACH
LONG BEACH, CALIFORNIA
90840

Contract N00014-77-0073

DECEMBER 1978

PREPARED FOR THE

OFFICE OF NAVAL RESEARCH ● 800 N. QUINCY ST. ● ARLINGTON ● VA ● 22217

REPORT ONR-CR297-002-1

THE CALCULATION OF MOMENTUM AND HEAT TRANSFER IN INTERNAL FLOWS AND IN FLOWS WITH SMALL REGIONS OF SEPARATION

TUNCER CEBECI

DEPARTMENT OF MECHANICAL ENGINEERING
CALIFORNIA STATE UNIVERSITY, AT LONG BEACH
LONG BEACH, CALIFORNIA
90840

Contract N00014-77-0073

DECEMBER 1978

PREPARED FOR THE

OFFICE OF NAVAL RESEARCH ● 800 N. QUINCY ST. ● ARLINGTON ● VA ● 22217

Unclassified

SECURITY CLASSIFICATION OF THIS PAGE (When Data Entered)

(19) REPORT DOCUMENTATION PAGE		READ INSTRUCTIONS BEFORE COMPLETING FORM
(18) 1. REPORT NUMBER ONR-CR297-002-1	2. GOVT ACCESSION NO.	3. RECIPIENT'S CATALOG NUMBER (9)
(6) 4. TITLE (and Subtitle) The Calculation of Momentum and Heat Transfer in Internal Flows and in Flows with Small Regions of Separation		5. TYPE OF REPORT & PERIOD COVERED Final Technical Report, Jan [redacted] — Dec [redacted] 1978
		6. PERFORMING ORG. REPORT NUMBER
(10) 7. AUTHOR(s) Tuncer/Cebeci		8. CONTRACT OR GRANT NUMBER(s) N00014-77-0073
9. PERFORMING ORGANIZATION NAME AND ADDRESS Department of Mechanical Engineering California State University, Long Beach Long Beach, California 90840		10. PROGRAM ELEMENT, PROJECT, TASK AREA & WORK UNIT NUMBERS (12) 71
11. CONTROLLING OFFICE NAME AND ADDRESS Office of Naval Research Department of the Navy Arlington, Virginia 22217		(11) 12. REPORT DATE December 1978
		13. NUMBER OF PAGES 66
14. MONITORING AGENCY NAME & ADDRESS (if different from Controlling Office) (15) N0014-77-C-0073		15. SECURITY CLASS. (of this report) Unclassified
		15a. DECLASSIFICATION/DOWNGRADING SCHEDULE

16. DISTRIBUTION STATEMENT (of this Report)

Distribution Unlimited

17. DISTRIBUTION STATEMENT (of the abstract entered in Block 20, if different from Report)

18. SUPPLEMENTARY NOTES

19. KEY WORDS (Continue on reverse side if necessary and identify by block number)

Laminar boundary layers
Turbulent boundary layers
Internal flows
Separating flows

20. ABSTRACT (Continue on reverse side if necessary and identify by block number)

Numerical methods for solving boundary-layer equations are discussed and the application of the Box scheme to internal flows and to small regions of separated flow is described in detail. The Box scheme has previously been used with considerable success to solve a wide range of external two- and three-dimensional flows and is shown here to be equally successful when applied in internal and separated flows which require its use in an inverse manner. A nonlinear eigenvalue and a Mechul method are described: the former is simpler

DD FORM 1 JAN 73 1473 EDITION OF 1 NOV 65 IS OBSOLETE S/N 0102-014-6601

Unclassified

SECURITY CLASSIFICATION OF THIS PAGE (When Data Entered)

409 265

to use and is recommended for internal flow problems; the latter is more appropriate for calculations in and through small regions of separated flow. Turbulent flow is characterized by eddy-viscosity and eddy-conductivity assumptions which are shown to represent the mean-flow and heat-transfer properties, including transition, provided the location of the onset of transition is known.

SUMMARY

Numerical methods for solving boundary-layer equations are discussed and the application of the Box scheme to internal flows and to small regions of separated flow is described in detail. The Box scheme has previously been used with considerable success to solve a wide range of external two- and three-dimensional flows and is shown here to be equally successful when applied in internal and separated flows which require its use in an inverse manner. A nonlinear eigenvalue and a Mechul method are described: the former is simpler to use and is recommended for internal flow problems; the latter is more appropriate for calculations in and through small regions of separated flow. Turbulent flow is characterized by eddy-viscosity and eddy-conductivity assumptions which are shown to represent the mean-flow and heat-transfer properties, including transition, provided the location of the onset of transition is known.

This report is based on the lectures given by the author in a conference on Turbulent Forced Convection in Channels and Rod Bundles held in Istanbul, Turkey, 20 July - 2 August 1978. The full proceedings of that conference will be published by Hemisphere Company.

TABLE OF CONTENTS

LIST OF FIGURES

NOTATION

A	Van Driest damping-length parameter
D	hydraulic diameter
F,f	dimensionless stream function
f'	u/u_o
L	reference length taken equal to r_o
Nu_x	local Nusselt number
p	local pressure
p_o	pressure at inlet to entrance section
Δp^*	dimensionless pressure drop $[\equiv(p_o - p)/(1/2)\rho u_o^2]$
P_o	pressure in reservoir upstream of inlet plane
Pr	Prandtl number
Pr_t	turbulent Prandtl number
r	radial distance from axis of revolution $(=r_o - y)$
r_o	pipe radius or half of channel width
R_D, R_L, R_x	Reynolds number $(=u_o D/\nu,\ u_o L/\nu,\ u_e X/\nu)$
R_θ	Reynolds number $(\equiv u_e \theta/\nu)$
St	local Stanton number
T	temperature
u,v	x- and y-component of velocity, respectively
u_c	centerline velocity
u_o	reference velocity taken equal to averaged velocity in duct
u_τ	shear velocity $(\equiv\sqrt{\tau_w/\rho})$
x	distance along body surface
x^{**}	dimensionless axial distance $(\equiv x R_D^{-1}/D)$
y	distance normal to x

y_c	centerline distance
δ	boundary-layer thickness
δ^*	displacement thickness $[\equiv \int_0^\infty (1 - u/u_e)dy]$
ε_m	eddy viscosity
ε_m^+	dimensionless eddy viscosity $(\equiv \varepsilon_m/\nu)$
η	transformed y-coordinate
η_L	value of η at centerline
θ	momentum thickness $[\equiv \int_0^\infty (u/u_e)(1 - u/u_e)dy]$
λ	parameter, see eq. (4.5)
γ_{tr}	intermittency
κ	Von Karman's constant
ν	kinematic viscosity
ρ	density
τ	shear stress

Subscripts

e	outer edge of boundary layer
tr	transition
w	wall
∞	freestream conditions

1.0 INTRODUCTION

The purpose of the present paper is to describe an efficient finite-difference method for the solution of the differential equations appropriate to thin shear layers, and representing conservation of mass, momentum and energy and to demonstrate that calculations of internal flows and flows with separation can be readily obtained. In a series of previous papers, see for example [1], Cebeci and coauthors have reported finite-difference solutions of boundary-layer equations for a range of boundary conditions corresponding to external boundary-layer flows. Essential features of the solution method have been the efficient and accurate numerical scheme of Keller [2] and, for turbulent flows, a simple eddy-viscosity formulation [1]. Previous applications have been mainly concerned with steady two-dimensional and axisymmetric flows [1], unsteady two-dimensional flows [3], steady three-dimensional flows [4] as well as with the solution of the stability equation for two-dimensional flows, namely, the Orr-Sommerfeld equation [5]. More recent developments have included the use of inverse methods which allow the calculation of internal-flow problems [6,7,8] and calculations through small regions of separated flow [9,10,11]. As a consequence of this previous work, the greater part of this report is concerned with the method described in reference 1 to 11 and its application to internal- and separated-flow problems.

A small number of calculated laminar-flow results for internal flows are presented and discussed. The emphasis is, however, on turbulent flows and on the extent of present ability to calculate from a laminar region, through transition, to a fully turbulent flow. The eddy-viscosity formulation, previously described by Cebeci and Smith [1] is a two-layer algebraic model. In its present form, it cannot be expected to represent three-dimensional

duct flows, but it is shown to allow the accurate calculation of developing turbulent two-dimensional plane- and round-duct flows. The energy equation is solved by the same numerical scheme, and, with the addition of a turbulent Prandtl number, allows correspondingly accurate results for heat transfer properties. Comparisons with measurements of heat-transfer information in a duct flow which undergoes transition from laminar to turbulent flow, confirms the validity of the model for this purpose.

Previous calculations of two-dimensional duct flows have, of course, been reported. Developing laminar flows have received considerable, and undeserved attention, as is indicated in section IV of this report and corresponding solutions to the energy equation have been reported, see for example Tien and Pawelek [12]. Developed turbulent-duct flow has also been considered in detail, for example, Na and Habib [13,14], and has successfully made use of a form of the present turbulence model. More recently, attention has turned to the solution of the momentum and energy equations for developing turbulent duct flow, for example, Nelson and Pletcher [15], Bradshaw, Dean and McEligot [16], and Emery and Gessner [17]. The present results demonstrate that two-dimensional duct flows in general, and including those which pass through transition from laminar to turbulent flow, can be represented by the present calculation procedure which combines accuracy with efficiency. Results are also presented for laminar and turbulent separated flows. It is well known that, for a prescribed external velocity distribution, the boundary-layer equations are singular at separation: they are not singular, however, when the displacement thickness is prescribed. This was demonstrated by Catherall and Mangler [18] who solved the laminar boundary-layer equations in the usual way until separation was approached and then, by assuming a displacement-thickness distribution,

calculated the external-velocity distribution and local flow properties through the recirculation region. More recent investigations of the inverse boundary-layer method have been reported, for example, by Klineberg and Steger [19], Horton [20], Carter [21,22], Carter and Wornom [23] and Williams [24,25], and have involved solutions to the laminar boundary-layer equations with prescribed displacement-thickness and shear-stress distributions in regions of negative shear stress. The present results, also obtained with the numerical procedure of references 1 to 10, are for laminar and turbulent flows where the external velocity distribution is known. They correspond to the laminar separating and reattaching flows previously calculated with Navier-Stokes equations by Briley [26] and Carter [22] and to the near-separating turbulent boundary-layer flows of Schubauer and Spangenberg (see Coles and Hirst, ref. 27). The results again demonstrate that the procedure of references 1 to 14, modified to operate in an inverse manner, allows accurate results with very small computer times.

The report has been prepared in three main sections. The following section states the basic equations and boundary conditions corresponding to the present range of flows; the equations are presented first in physical coordinates and then in transformed coordinates, appropriate to boundary-layer flows. Numerical methods are reviewed in the first subsection of Section 3 and alternative approaches to internal-flow problems, making use of the numerical scheme of references 1 to 14, are described in subsections 3.2 and 3.3. The nonlinear eigenvalue approach of section 3.2 is simpler than the alternative Mechul function approach of section 3.3 and is preferred for internal-flow calculations. The Mechul method is, however, also appropriate to internal and external flows with separation, and its application to separated external flows is described in subsection 4.5. The solution of

the energy equation, for internal flows, is considered in section 3.4. The results are presented in section 4 which emphasizes the capabilities of the eddy-viscosity formulation for turbulent flows and of the numerical schemes. A closing section presents brief conclusions.

2.0 BASIC EQUATIONS AND BOUNDARY CONDITIONS

The equations used to characterize the flow configurations of section 4 may be written in the form

Continuity

$$\frac{\partial}{\partial x}(r^k u) + \frac{\partial}{\partial y}(r^k v) = 0 \tag{2.1}$$

Momentum

$$u\frac{\partial u}{\partial x} + v\frac{\partial u}{\partial y} = -\frac{1}{\rho}\frac{dp}{dx} + \frac{\nu}{r^k}\frac{\partial}{\partial y}\left[r^k(1+\varepsilon_m^+)\frac{\partial u}{\partial y}\right] \tag{2.2}$$

Energy

$$u\frac{\partial T}{\partial x} + v\frac{\partial T}{\partial y} = \frac{\nu}{Pr}\frac{1}{r^k}\frac{\partial}{\partial y}\left[r^k\left(1+\frac{Pr}{Pr_t}\varepsilon_m^+\right)\frac{\partial T}{\partial y}\right] \tag{2.3}$$

They represent, respectively, conservation of mass, momentum and energy for two-dimensional boundary-layer flows where variations in density and specific heat are unimportant. For turbulent flows, they presume that the diffusion of momentum and energy may be represented by an effective viscosity and Prandtl number, respectively: the specific assumptions used here are introduced and discussed in section 4. The flow index, k, is zero for plane flow and unity for axisymmetric flow.

The parabolic nature of the thin shear-layer (TSL) equations requires that boundary conditions be provided on three sides of the solution domain. In addition to initial conditions for the momentum and energy equations, the zero slip condition requires that the u-velocity be zero at the wall and the wall temperature or heat-flux may be prescribed according to the problem to be solved.

Equations (2.1) to (2.3) may be solved in the forms presented above or may be transformed, for a particular problem, to allow solutions with improved economy and accuracy.

2.1 Internal Flows

For internal flows, where a symmetry condition usually provides the third boundary condition, it is convenient to transform the equations to the Falkner-Skan form [28] to obtain solutions in regions where the boundary-layer thickness is less than half the duct width. Where the boundary-layer fills the duct, physical coordinates are desirable. In the present calculations, the change from transformed to physical coordinates is made when the boundary-layer thickness becomes approximately 0.75 of the half-width of the duct.

It is convenient to nondimensionalize equations (2.1) to (2.3) and, for solutions in transformed variables, to introduce Mangler's transformation and the stream function. The introduction of the dimensionless quantities

$$p^* = \frac{p}{\rho u_o^2}, \quad u^* = \frac{u}{u_o}, \quad v^* = \frac{v}{u_o}\sqrt{R_L}, \quad y^* = \frac{y}{L}\sqrt{R_L}, \quad x^* = \frac{x}{L}, \quad r^* = \frac{r}{L}$$

$$R_L = \frac{u_o L}{\nu}, \qquad g = \frac{T}{T_o} \tag{2.4}$$

allows equations (2.1) to (2.3) to be expressed as:

$$\frac{\partial}{\partial x^*}\left[(r^*)^k u^*\right] + \frac{\partial}{\partial y^*}\left[(r^*)^k v^*\right] = 0 \tag{2.5}$$

$$u^* \frac{\partial u^*}{\partial x^*} + v^* \frac{\partial u^*}{\partial y^*} = -\frac{dp^*}{dx^*} + \frac{1}{(r^*)^k}\frac{\partial}{\partial y^*}\left(b_1 \frac{\partial u^*}{\partial y^*}\right) \tag{2.6}$$

$$u^* \frac{\partial g}{\partial x^*} + v^* \frac{\partial g}{\partial y^*} = \frac{1}{Pr}\frac{1}{(r^*)^k}\frac{\partial}{\partial y^*}\left(b_2 \frac{\partial g}{\partial y^*}\right) \tag{2.7}$$

where

$$b_1 = (r^*)^k(1 + \varepsilon_m^+), \qquad b_2 = (r^*)^k(1 + Pr/Pr_t\ \varepsilon_m^+) \tag{2.8}$$

The Mangler transformation

$$d\bar{x} = (r_o^*)^{2k}dx^*, \qquad d\bar{y} = (r^*)^k dy^* \tag{2.9}$$

ensures that equations (2.5) to (2.7) have a form which is common to plane and axisymmetric flows, i.e.

$$\frac{\partial \bar{u}}{\partial \bar{x}} + \frac{\partial \bar{v}}{\partial \bar{y}} = 0 \tag{2.10}$$

$$\bar{u}\,\frac{\partial \bar{u}}{\partial \bar{x}} + \bar{v}\,\frac{\partial \bar{u}}{\partial \bar{y}} = -\frac{dp^*}{d\bar{x}} + \frac{\partial}{\partial \bar{y}}\left(b_1\,\frac{\partial \bar{u}}{\partial \bar{y}}\right) \tag{2.11}$$

$$\bar{u}\,\frac{\partial g}{\partial \bar{x}} + \bar{v}\,\frac{\partial g}{\partial \bar{y}} = \frac{1}{Pr}\,\frac{\partial}{\partial \bar{y}}\left(b_2\,\frac{\partial g}{\partial \bar{y}}\right) \tag{2.12}$$

Here $\bar{u}$ and $\bar{v}$ are related to u^* and v^* through

$$u^* = \bar{u}, \qquad v^* = -\frac{(r_o^*)^{2k}}{(r^*)^k}\,\bar{v} - \frac{\bar{u}}{(r^*)^k}\,\frac{d\bar{y}}{dx^*} \tag{2.13}$$

Introducing the stream function, defined as

$$\bar{u} = \frac{\partial F}{\partial \bar{y}}, \qquad \bar{v} = -\frac{\partial F}{\partial \bar{x}} \tag{2.14}$$

equations (2.10) to (2.12) may be rewritten as

$$(b_1 F'')' = \frac{dp^*}{d\bar{x}} + F'\,\frac{\partial F'}{\partial \bar{x}} - F''\,\frac{\partial F}{\partial \bar{x}} \tag{2.15}$$

$$(b_2 g')' = Pr\left(F'\,\frac{\partial g}{\partial \bar{x}} - g'\,\frac{\partial F}{\partial \bar{x}}\right) \tag{2.16}$$

Here primes denote differentiation with respect to $\bar{y}$.

Equations (2.15) and (2.16) may be rewritten in the transformed variables $\bar{x}$ and η by introducing the Falkner-Skan variable.

$$\eta = \bar{y}/\sqrt{\bar{x}} \tag{2.17a}$$

and the modified stream function

$$F(\bar{x},\bar{y}) = \sqrt{\bar{x}}\, f(\bar{x},\eta) \tag{2.17b}$$

Thus

$$(b_1 f'')' + \frac{1}{2} ff'' = \bar{x}\left(\frac{dp^*}{d\bar{x}} + f' \frac{\partial f'}{\partial \bar{x}} - f'' \frac{\partial f}{\partial \bar{x}}\right) \tag{2.18}$$

$$(b_2 g')' + \frac{1}{2} Pr\, fg' = Pr\, \bar{x}\left(f' \frac{\partial g}{\partial \bar{x}} - g' \frac{\partial f}{\partial \bar{x}}\right) \tag{2.19}$$

where the primes now represent differentiation with respect to η. The parameters b_1 and b_2 may also be rewritten with r^* given by

$$r^* = r_o^* \left(1 - \frac{2\bar{y}}{r_o^{*2}\sqrt{R_L}}\right)^{1/2} = r_o^* \left(1 - 2\frac{\sqrt{\bar{x}}\eta}{r_o^{*2}\sqrt{R_L}}\right)^{1/2} \tag{2.20}$$

When the governing equations are solved in transformed variables, the boundary conditions are specified at the wall and at the edge of the boundary layer. For the case of no mass transfer, they are given by:

$$y = 0, \quad u = 0, \quad v = 0, \quad aT_w(x) + bT_w'(x) = \text{given} \tag{2.21a}$$

$$y = \delta, \quad u = u_e, \quad T = T_\infty \tag{2.21b}$$

Here $a = 0$ corresponds to the case in which wall heat flux is specified and $b = 0$ corresponds to specified wall temperature. When the governing equations

are solved in physical variables, the boundary conditions are specified at one wall and at the centerline of the duct provided both surfaces are kept at the same temperature. Otherwise the centerline boundary conditions must be replaced by those on the other wall, similar to those in (2.21a) except with different $T_w(x)$. For the case when we use the boundary conditions on the centerline $y = y_c$,

$$y = y_c, \qquad \frac{\partial u}{\partial y} = 0, \qquad \frac{\partial T}{\partial y} = 0 \tag{2.22}$$

In terms of dimensionless quantities, equations (2.21) and (2.22) can be written as

Wall boundary conditions

$$\eta = 0 \qquad f = f' = 0, \qquad \tilde{a}g_w(x) + \tilde{b}g_w'(x) = \text{given} \tag{2.23a}$$

$$\bar{y} = 0 \qquad F = F' = 0 \qquad \tilde{a}g_w(x) + \tilde{b}g_w'(x) = \text{given} \tag{2.23b}$$

Boundary-layer edge conditions

$$\eta = \eta_\infty \qquad \frac{d}{d\bar{x}} \frac{(f')^2}{2} = -\frac{dp^*}{d\bar{x}} \tag{2.24}$$

Centerline boundary conditions

$$\bar{y} = \sqrt{R_L} \qquad f'' = 0 \qquad g' = 0 \tag{2.25}$$

The presence of the $dp^*/d\bar{x}$ term in either equation (2.15) or (2.18) introduces an additional unknown to the system given by (2.15), (2.16), (2.23b) and (2.24) or by (2.18), (2.19), (2.23a) and (2.25). Thus, another equation is needed and is provided by the conservation of mass in integral form. In the case of a <u>two-dimensional duct with constant cross section</u>, mass balance gives

$$u_o L = \int_0^L u dy \tag{2.26}$$

Here L corresponds to the half-width of the duct. In terms of dimensionless variables and stream function expressed in physical coordinates, equation (2.26) can be written as

$$F(x, \sqrt{R_L}) = \sqrt{R_L} \tag{2.27}$$

When the stream function is expressed in transformed variables, equation (2.26) can be written in a form similar to equation (2.27), i.e.

$$f(\bar{x}, \eta_L) = \sqrt{R_L}/\bar{x} \tag{2.28}$$

Similarly, for the case of a circular pipe, relations similar to (2.27) and (2.28) can be written as

$$F(\bar{x}, \sqrt{R_L}) = \frac{1}{2}\sqrt{R_L} \tag{2.29}$$

and

$$f(\bar{x}, \eta_L) = \frac{1}{2}\sqrt{R_L}/\bar{x} \tag{2.30}$$

2.2 Separated Flows

As is well known, for a given external velocity distribution the governing TSL equations become singular at separation. This occurs when wall shear is equal to zero. To continue the calculations into the region of negative wall shear, it is necessary to prescribe an alternative boundary condition, such as wall shear or displacement thickness and to treat the external velocity or pressure as an unknown. According to the Mechul method, to be described in section 3.3, separated flow calculations for external flows can be achieved by solving the TSL equations subject to the following boundary conditions:

$$
\begin{aligned}
&y = 0 \qquad && u = v = 0 \\
&y = \delta \qquad && u = u_e \qquad && \delta^*(x) = \text{given}
\end{aligned}
\tag{2.31}
$$

Since the displacement thickness is not known in the separated flow region a priori, it is assumed and the external velocity distribution is computed for the prescribed displacement thickness distribution. This procedure is repeated until convergence is achieved.

For internal flows, the displacement thickness is specified by conservation of mass. Therefore, when flow separation occurs, the calculations are simpler than for external flows. When the governing equations are expressed in transformed coordinates for a two-dimensional duct with constant cross section, we solve them subject to the following boundary conditions:

$$
\begin{aligned}
&\eta = 0 \qquad && f = f' = 0 \\
&\eta = \eta_L \qquad && f = \sqrt{R_L}/x, \qquad && f' = u_e
\end{aligned}
\tag{2.32}
$$

When the governing equations are expressed in physical coordinates, the boundary conditions become

$$
\begin{aligned}
&y^* = 0 \qquad && F = F' = 0 \\
&y^* = \sqrt{R_L} \qquad && F = \sqrt{R_L}\,, \qquad && F'' = 0
\end{aligned}
\tag{2.33}
$$

3.0 NUMERICAL METHODS

The purpose of this section is to describe numerical methods for the solution of the parabolic, thin-shear-layer form of the momentum and energy equations. In the following subsection, a brief review of appropriate numerical methods is presented and the relative advantages of implicit and explicit finite-difference methods is discussed. As a result, the Box scheme is preferred and is described in detail in relation to the momentum equation. The application of the Box scheme to the solution of the internal flow problem of interest here is described in the following two subsections which are concerned with a "nonlinear eigenvalue" and the "Mechul" approach, respectively: both methods were developed by Keller and Cebeci, see, for example references 6 and 9. In the former approach, the pressure is regarded as an eigenvalue parameter and in the latter as an unknown function. As indicated in reference 9, the Mechul approach has the advantage of allowing solutions in regions of flow recirculation but the nonlinear eigenvalue method is simpler to use. The penultimate subsection describes the solution of the energy equation and the section ends with brief comments on the solution algorithm.

3.1 A Brief Review of Numerical Methods for TSL Equations

Various methods for solving TSL equations have been described in reference 28 and include finite-difference methods, method of lines, Galerkin method and finite-element methods. Of these methods, the finite-difference methods are much more appropriate to solve the TSL equations and, as a consequence, only finite-difference methods are considered here.

To illustrate the application of finite-difference methods to parabolic equations, it is useful to consider the unsteady, one-dimensional equation, appropriate to the Rayleigh problem and to heat conduction, i.e.

$$\frac{\partial u}{\partial t} = \frac{\partial^2 u}{\partial x^2} \qquad 0 \leq x \leq L \tag{3.1}$$

The solution of (3.1), as in any partial-differential equation, requires initial and boundary conditions, which serve to complete the formulation of a "meaningful" problem. Let us assume that they are given by

Boundary conditions

$$\begin{aligned} x &= 0 \qquad u = \text{given} \\ x &= L \qquad u = \text{given} \end{aligned} \tag{3.2a}$$

Initial conditions

$$t = 0 \qquad u = u(x) = \text{given} \tag{3.2b}$$

The solution of (3.1) by a finite-difference method requires that we approximate the derivatives by some difference approximations. Using Taylor's theorem and requiring that the function u and its derivatives are single-valued, finite and continuous functions of x, we can write

$$u(x + h) = u(x) + hu'(x) + \frac{1}{2} h^2 u''(x) + \frac{1}{6} h^3 u'''(x) + \ldots \tag{3.3a}$$

and

$$u(x - h) = u(x) - hu'(x) + \frac{1}{2} h^2 u''(x) - \frac{1}{6} h^3 u'''(x) + \ldots \tag{3.3b}$$

Adding (3.3a) and (3.3b) we get

$$u(x + h) + u(x - h) = 2u(x) + h^2 u''(x)$$

provided the fourth and higher-order terms are neglected. Thus,

$$u''(x) = \frac{1}{h^2} [u(x + h) - 2u(x) + u(x - h)] \tag{3.4}$$

with an error of order h^2.

If (3.3b) is subtracted from (3.3a)

$$u'(x) = \frac{1}{2h} [u(x + h) - u(x - h)] \tag{3.5}$$

Equation (3.5) approximates the slope of the tangent at P by the slope of the chord AB (see figure 1) and is called a central-difference approximation. The slope of the tangent at P can also be approximated by either the slope of the chord PB, giving the forward-difference formula

$$u'(x) = \frac{1}{h}\left[u(x + h) - u(x)\right] \tag{3.6}$$

or the slope of the chord AP giving the backward-difference formula

$$u'(x) = \frac{1}{h}\left[u(x) - u(x - h)\right] \tag{3.7}$$

Note that while (3.5) is of $O(h^2)$, both (3.6) and (3.7) are of $O(h)$.

To demonstrate finite-difference notation, figure 2 indicates a set of net points on the x-t plane, i.e.

$$\begin{aligned} x_i &= x_o + ih, \qquad i = 0, 1, 2, \ldots I \\ \text{and} \qquad t_j &= t_o + jk, \qquad j = 0, 1, 2, \ldots J \end{aligned} \tag{3.8}$$

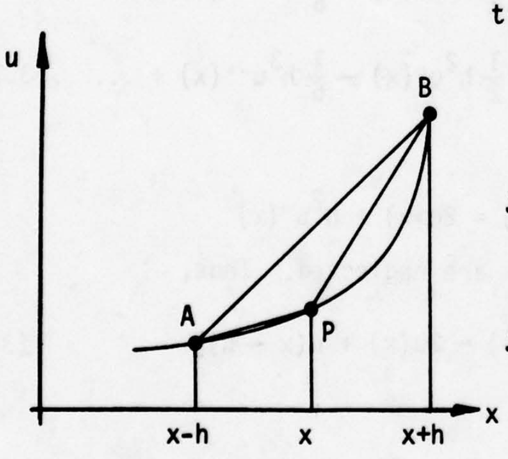

Figure 1. Notation for approximation of derivatives.

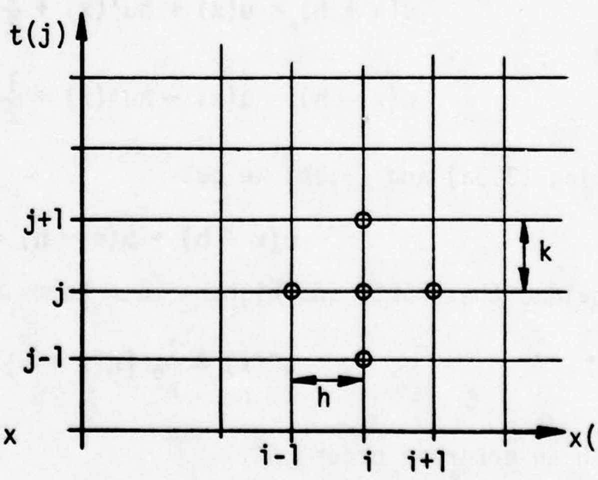

Figure 2. General finite-difference grid notation.

where h and k are the distance and time mesh width, respectively. With

$$u(t_j, x_i) = u_i^j \tag{3.9}$$

the difference approximations of equations (3.4) to (3.7) may be written as

$$u'(x_i^j) = \begin{cases} = \frac{1}{2h}\left[u_{i+1}^j - u_{i-1}^j\right] & \text{central difference from (3.5)} \\ = \frac{1}{h}\left[u_{i+1}^j - u_i^j\right] & \text{forward difference from (3.6)} \\ = \frac{1}{h}\left[u_i^j - u_{i-1}^j\right] & \text{backward difference from (3.7)} \end{cases} \tag{3.10}$$

$$u''(x_i^j) = \frac{1}{h^2}\left[u_{i+1}^j - 2u_i^j + u_{i-1}^j\right] \tag{3.11}$$

The solution of (3.1) may be obtained by using either an explicit or an implicit method. In the former, the value of u at the downstream station is *expressed in terms of upstream quantities* and the corresponding equation can be solved explicitly: in the latter, u at the downstream station is expressed in terms of its downstream neighbors and the known upstream quantities.

An explicit formulation may be obtained by representing $\partial u/\partial t$ by the forward-difference example of (3.10) and $\partial^2 u/\partial x^2$ by (3.11), both at the net point (x_i, t_j) as indicated in figure 3; i.e.

$$\frac{u_i^{j+1} - u_i^j}{k} = \frac{1}{h^2}\left[u_{i+1}^j - 2u_i^j + u_{i-1}^j\right] \tag{3.12}$$

or

$$u_i^{j+1} = u_i^j + \frac{k}{h^2}\left[u_{i-1}^j - 2u_i^j + u_{i+1}^j\right], \qquad i = 1, 2, 3, \ldots I \tag{3.13}$$

Equation (3.12) provides an explicit finite-difference approximation to (3.1) centered at the net point (x_i, t_j). The value of u_i^{j+1} is expressed in terms of

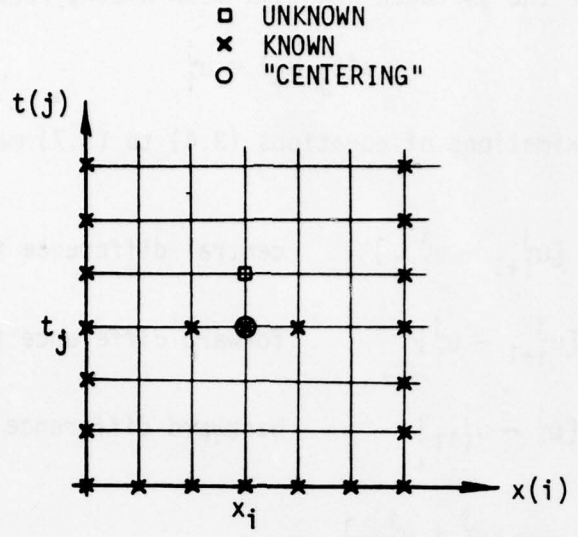

Figure 3. Finite-difference grid for an explicit method.

upstream values which are known and the equation allows the value of u to be obtained at all values of t_{j+1}. The numerical error inherent in this scheme can be shown to be of order $(k + h^2)$ and, as a result the x-step, h, must be maintained small to ensure acceptable accuracy. In addition, and although explicit formulations are computationally simple, they can lead to instabilities unless the time step is also small; in this connection it is necessary to ensure that $k < 1/2\ h^2$.

In contrast, implicit methods do not have stability requirements and significantly larger time steps, with corresponding economy, can be taken. As an example, the Crank-Nicholson [29] approach replaces $\partial^2 u/\partial x^2$ by the means of the finite-difference approximations at $(x_i, t_{j-1/2})$; i.e.

$$\frac{\partial^2 u}{\partial x^2} = \frac{1}{2}\left[\left(\frac{\partial^2 u}{\partial x^2}\right)_i^{j+1} + \left(\frac{\partial^2 u}{\partial x^2}\right)_i^{j}\right]$$

and, with the central-difference form of (3.10) (figure 4) leads to

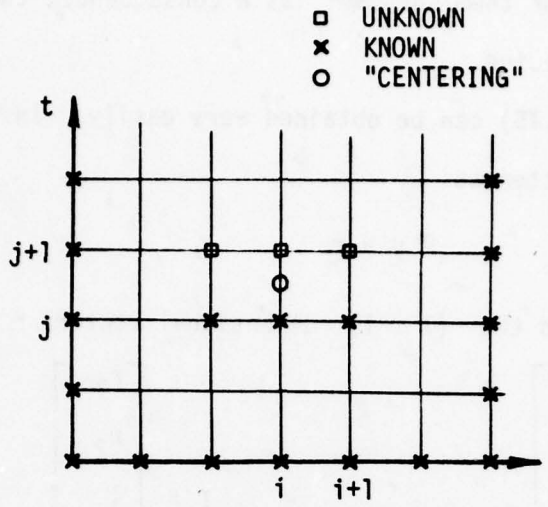

Figure 4. Finite-difference grid for Crank-Nicholson method.

$$\frac{u_i^{j+1} - u_i^j}{k} = \frac{1}{2}\left[\frac{u_{i+1}^{j+1} - 2u_i^{j+1} + u_{i-1}^{j+1}}{h^2} + \frac{u_{i+1}^{j} - 2u_i^{j} + u_{i-1}^{j}}{h^2}\right]$$

Equation (3.14) can be rewritten in the form:

$$a_i u_{i-1}^{j+1} + b_i u_i^{j+1} + c_i u_{i+1}^{j+1} = r_i \qquad 1 \le i \le I-1 \qquad (3.14)$$

where

$$a_i = -\frac{k}{h^2}, \qquad b_i = 2\left(1 + \frac{k}{h^2}\right), \qquad c_i = -\frac{k}{h^2}$$

$$r_i = \frac{k}{h^2} u_{i-1}^j + 2\left(1 - \frac{k}{h^2}\right)u_i^j + \frac{k}{h^2} u_{i+1}^j \qquad (3.15)$$

The errors in this carefully centered scheme are of order $(h^2 + k^2)$ but k need not be related to h for stability purposes. The scheme is unconditionally stable and second-order accuracy may be achieved with uniform x-spacing. On the other hand, the unknown value of u is expressed in terms of five other

values of u with two of them unknown: as a consequence, the computational arithmetic is more extensive.

The solution of (3.15) can be obtained very easily. In vector notation, the equation may be written as

$$A \underset{\sim}{u} = \underset{\sim}{r} \tag{3.16}$$

where we have introduced the $(I-1)$ dimensional vectors

$$\underset{\sim}{u} \equiv \begin{bmatrix} u_1 \\ u_2 \\ \vdots \\ u_{I-1} \end{bmatrix} \qquad \underset{\sim}{r} \equiv \begin{bmatrix} r_1 \\ r_2 \\ \vdots \\ r_{I-1} \end{bmatrix} \tag{3.17a}$$

and the (I-1)-order matrix (called tridiagonal matrix)

$$A = \begin{bmatrix} b_1 & c_1 & & & \\ a_2 & b_2 & c_2 & & \\ & \ddots & \ddots & \ddots & \\ & & a_{I-2} & b_{I-2} & c_{I-2} \\ & & & a_{I-1} & b_{I-1} \end{bmatrix} \tag{3.17b}$$

Then the solution of (3.16) is obtained by two sweeps. In the so-called forward sweep, the following are determined;

$$\begin{aligned} \beta_1 &= b_1, & \gamma_1 &= c_1/\beta_1 \\ \beta_i &= b_i - a_i\gamma_{i-1} & i &= 2, 3, \ldots, I-1 \\ \gamma_i &= c_i/\beta_i & i &= 2, 3, \ldots, I-2 \end{aligned} \tag{3.18a}$$

In the backward-sweep,

$$z_1 = r_1/\beta_1, \qquad z_i = (r_i - a_i z_{i-1})/\beta_i \qquad i = 2, 3, \ldots, I-1$$
$$u_{I-1} = z_{I-1} \qquad u_i = z_i - \gamma_i u_{i+1} \qquad i = I-2, I-3, \ldots, 1 \tag{3.18b}$$

are obtained.

An alternative implicit method due to H.B. Keller [2] and Keller and Cebeci [6] is now described and is referred to as the Box method. This method has several very desirable features that make it appropriate for the solution of all parabolic partial-differential equations as discussed by Cebeci and Bradshaw [28] and Keller [30]. The main features of this method are:

1. slightly more arithmetic to solve,
2. second-order accuracy with arbitrary (nonuniform) x-spacing,
3. allows very rapid x-variations.

The solution of a parabolic partial-differential equations by the Box method require the following four steps:

1. reduce the governing equations to a first-order system,
2. write difference equations using central differences,
3. linearize the resulting algebraic equations (if they are nonlinear) and write them in matrix-vector form,
4. solve the linear system by the block tridiagonal elimination method.

Reverting to the notation of section 2, equations (3.1) and (3.2a) may be written as:

$$\frac{\partial u}{\partial x} = \frac{\partial^2 u}{\partial y^2} = u'' \tag{3.19}$$

$$y = 0, \quad u = a; \qquad y = L, \quad u = b \tag{3.20}$$

To allow (3.19) to be written as a first-order system,

$$u' = v \tag{3.21a}$$

$$v' = \frac{\partial u}{\partial x} \tag{3.21b}$$

and the difference equations may be written to approximate (3.20) with (3.21a) centered at P_1P_2 $(x_i, y_{j-1/2})$ (see the rectangle of figure 5) to get;

$$\frac{u_j^i - u_{j-1}^i}{h_{j-1}} = v_{j-1/2}^i \tag{3.22}$$

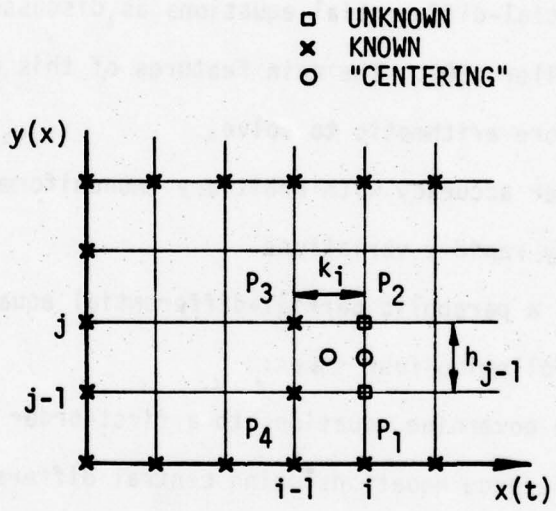

Figure 5. Finite-difference grid for the Box scheme.

The difference form of (3.21b) can be obtained by centering at the middle of $P_1P_2P_3P_4$ $(x_{i-1/2}, y_{j-1/2})$ as follows. Center (3.21b) at $x_{i-1/2}$ to obtain

$$\frac{(v')^i + (v')^{i-1}}{2} = \frac{u^i - u^{i-1}}{k_i} \tag{3.23a}$$

Equation (3.23a) can also be written as

$$(v')^i - \frac{2}{k_i} u^i = -(v')^{i-1} - \frac{2}{k_i} u^{i-1} \equiv R^{i-1} \tag{3.23b}$$

In the second step equation (3.23b) is centered at $y_{j-1/2}$ to obtain

$$v_j^i - v_{j-1}^i - \frac{h_{j-1}}{k_i}(u_j^i + u_{j-1}^i) = h_{j-1} R_{j-1/2}^{i-1} \qquad (3.23c)$$

Here

$$R_{j-1/2}^{i-1} = -\frac{v_j^{i-1} - v_{j-1}^{i-1}}{h_{j-1}} - \frac{2}{k_i} u_{j-1/2}^{i-1}$$

$$u_{j-1/2}^{i-1} = \frac{u_j^{i-1} + u_{j-1}^{i-1}}{2} \quad , \quad v_{j-1/2}^{i} = \frac{(v_j^i + v_{j-1}^i)}{2}$$

Since (3.23c) is linear, as are the corresponding boundary conditions, the system may be written in matrix-vector form as shown below.

$$\begin{array}{l|cccccc|c|c}
 & u_0 & v_0 & u_j & v_j & u_J & v_J & & \\
\text{b.c.} \longrightarrow & 1 & 0 & 0 & 0 & & & \begin{pmatrix} u_0 \\ v_0 \end{pmatrix} & \begin{pmatrix} (r_1)_0 \\ (r_2)_0 \end{pmatrix} \\
\text{eq.(3.24c)} & -1 & \frac{-h_0}{2} & 1 & \frac{-h_0}{2} & & & & \\
\text{eq.(3.23)} & \frac{-h_{j-1}}{k_i} & -1 & \frac{-h_{j-1}}{k_i} & 1 & 0 & 0 & \begin{pmatrix} u_j \\ v_j \end{pmatrix} & = \begin{pmatrix} (r_1)_j \\ (r_2)_j \end{pmatrix} \\
 & 0 & 0 & -1 & \frac{-h_j}{2} & 1 & \frac{-h_j}{2} & & \\
 & & & \frac{-h_{J-1}}{k_i} & -1 & \frac{-h_{J-1}}{k_i} & 1 & \begin{pmatrix} u_J \\ v_J \end{pmatrix} & \begin{pmatrix} (r_1)_J \\ (r_2)_J \end{pmatrix} \\
\text{b.c.} \longrightarrow & & & 0 & 0 & 1 & 0 & &
\end{array} \qquad (3.24)$$

where

$$(r_1)_0 = a \qquad (r_1)_j = h_{j-1} R_{j-1/2}^{i-1} \qquad 1 \le j \le J$$

$$(r_2)_j = 0 \qquad 0 \le j \le J-1 \qquad (r_2)_J = b$$

This equation may be rewritten as:

$$A\,\xi = r \qquad (3.25)$$

where

$$\mathbf{A} \equiv \begin{bmatrix} A_0 & C_0 & & & & \\ B_1 & A_1 & C_1 & & & \\ & B_j & A_j & C_j & & \\ & & B_{J-1} & A_{J-1} & C_{J-1} & \\ & & & B_J & A_J & \end{bmatrix} \qquad \delta = \begin{bmatrix} \delta_0 \\ \delta_1 \\ \vdots \\ \delta_j \\ \vdots \\ \delta_J \end{bmatrix} \qquad r = \begin{bmatrix} r_0 \\ r_1 \\ \vdots \\ r_j \\ \vdots \\ r_J \end{bmatrix} \tag{3.26}$$

$$\delta_j = \begin{pmatrix} u_j \\ v_j \end{pmatrix} \qquad r_j = \begin{pmatrix} (r_1)_j \\ (r_2)_j \end{pmatrix} \tag{3.27a}$$

and A_j, B_j, C_j are 2x2 matrices defined as follows:

$$A_0 \equiv \begin{pmatrix} 1 & 0 \\ -1 & \frac{-h_0}{2} \end{pmatrix} \quad C_j \equiv \begin{pmatrix} 0 & 0 \\ 1 & \frac{-h_j}{2} \end{pmatrix} \quad 0 \le j \le J-1, \quad A_J \equiv \begin{pmatrix} \frac{-h_J}{k_1} & 1 \\ 1 & 0 \end{pmatrix}$$

$$B_j \equiv \begin{pmatrix} \frac{-h_{j-1}}{k_i} & -1 \\ 0 & 0 \end{pmatrix} \quad 1 \le j \le J, \quad A_j \equiv \begin{pmatrix} \frac{-h_{j-1}}{k_i} & 1 \\ -1 & \frac{-h_j}{2} \end{pmatrix} \quad 1 \le j \le J-1 \tag{3.27b}$$

Note that, as in the Crank Nicholson method, the implicit nature of the method has again generated a tridiagonal matrix, but with 2x2 blocks rather than scalars.

The solution of (3.25) is obtained by the block elimination method discussed by Keller [31] and by Cebeci and Bradshaw [28]. This method consists of two sweeps. In the forward sweep we compute Γ_j, Δ_j and $\underset{\sim}{W}_j$ from the following recursion formulas

$$\left.\begin{aligned} \Delta_0 &= A_0 \\ \Gamma_j \Delta_{j-1} &= B_j \\ \Delta_j &= A_j - \Gamma_j C_{j-1} \end{aligned}\right\} \qquad 1 \le j \le J$$

$$\left.\begin{aligned} \underset{\sim}{W}_0 &= \underset{\sim}{r}_0 \\ \underset{\sim}{W}_j &= \underset{\sim}{r}_j - \Gamma_j \underset{\sim}{W}_{j-1} \end{aligned}\right\} \qquad 1 \le j \le J \tag{3.28}$$

Here Γ_j has the same structure as B_j, that is,

$$\Gamma_j \equiv \begin{pmatrix} (\alpha_{11})_j & (\alpha_{12})_j \\ 0 & 0 \end{pmatrix}$$

and the second row of Δ_j is the same as the second row of A_j,

$$\Delta_j \equiv \begin{pmatrix} (\alpha_{11})_j & (\alpha_{12})_j \\ -1 & -\frac{h_j}{2} \end{pmatrix}$$

In the backward sweep, $\underset{\sim}{\delta}_j$ is computed from the following recursion formulas:

$$\begin{aligned} \Delta_j \underset{\sim}{\delta}_J &= \underset{\sim}{W}_J \\ \Delta_j \underset{\sim}{\delta}_j &= \underset{\sim}{W}_j - C_j \underset{\sim}{\delta}_{j+1} \qquad j = J-1, J-2, \ldots, 0 \end{aligned} \tag{3.29}$$

For further details, the reader is referred to Cebeci and Bradshaw [28].

3.2 Momentum Equation and the Nonlinear Eigenvalue Method for Internal Flows

In the mathematical description of an internal boundary-layer flow, the geometry rather than the pressure distribution is known. Thus, the solution of (2.18) requires a form of iteration to determine $dp^*/d\bar{x}$. In the nonlinear eigenvalue approach, this situation is performed by applying Newton's method

to the solution of the nonlinear algebraic equations corresponding to a finite-difference form of equation (2.18). This equation is solved first with an assumed pressure gradient in the manner usually applied to the external boundary-layer problem, for brevity referred to here as the standard problem; the next values of dp* are obtained by applying Newton's method. For example, rewritting dp* by $-\beta$ and equation (2.28) as

$$\phi(\beta^{\nu}) \equiv f(x,\eta_L) - \eta_L \tag{3.30}$$

then the next value of $\beta^{\nu+1}$ is obtained from

$$\beta^{\nu+1} = \beta^{\nu} - \frac{\phi(\beta^{\nu})}{\partial/\partial\beta[\phi(\beta^{\nu})]} \qquad \nu = 0, 1, 2, \ldots \tag{3.31}$$

The derivative of ϕ with respect to β is obtained from equation (3.30), i.e.

$$\frac{\partial}{\partial\beta}[\phi(\beta^{\nu})] = \frac{\partial}{\partial\beta}[f(\bar{x},\eta_L)] \tag{3.32}$$

The derivative of f with respect to β is obtained by solving a system of variational equations to be described later in this subsection. The iteration process is repeated until

$$|\beta^{\nu+1}(\bar{x}) - \beta^{\nu+1}(\bar{x})| < \varepsilon_1 \tag{3.33}$$

where ε_1 is a small error tolerance which may be specified.

The standard problem and the variational equations, described in detail below, are solved with the two-point finite-difference method developed by Keller [2]. The application of the standard problem to two- and three-dimensional boundary layers is described in detail in reference 28 and only a brief outline is provided here.

In accordance with Keller's Box scheme, the new dependent variables $u(\bar{x},\eta)$ and $v(\bar{x},\eta)$ are introduced and allow equation (2.18) to be written as the first-order system,

$$f' = u \tag{3.34a}$$

$$u' = v \tag{3.34b}$$

$$(b_1 v)' + \frac{1}{2} fv = \bar{x}\left(\frac{dp^*}{d\bar{x}} + u\frac{\partial u}{\partial \bar{x}} - v\frac{\partial f}{\partial \bar{x}}\right) \tag{3.34c}$$

On $0 \le \bar{x} \le \bar{x}_N$, $0 \le \eta \le \eta_\infty$, we place a possibly nonuniform net:

$$\begin{aligned} &\bar{x}_0 = 0, && \bar{x}_n = \bar{x}_{n-1} + k_n && n = 1, 2, \ldots, N \\ &\eta_0 = 0, && \eta_j \equiv \eta_{j-1} + h_j && j = 1, 2, \ldots, J \quad \eta_J = \eta_\infty \end{aligned} \tag{3.35}$$

with k_n and h_j denoting variable distances between nodes in the $\bar{x}$ and η directions. The finite-difference forms of equations (3.34a) and (3.34b), with central-difference quotients and averages about the midpoint $(\bar{x}_n, \eta_{j-1/2})$, then can be written as

$$h_j^{-1}(f_j^n - f_{j-1}^n) = u_{j-1/2}^n \tag{3.36a}$$

$$h_j^{-1}(u_j^n - u_{j-1}^n) = v_{j-1/2}^n \tag{3.36b}$$

Similarly equation (3.34c) is approximated by centering about the midpoint $(\bar{x}_{n-1/2}, \eta_{j-1/2})$ of a rectangle whose mesh widths are k_n and h_j:

$$\begin{aligned} &h_j^{-1}[(b_1 v)_j^n - (b_1 v)_{j-1}^n] - \alpha_n (u^2)_{j-1/2}^n + \frac{1}{2} + \alpha_n (fv)_{j-1/2}^n \\ &\quad + \alpha_n [f_{j-1/2}^n v_{j-1/2}^{n-1} - v_{j-1/2}^n f_{j-1/2}^{n-1}] = T_{j-1/2}^{n-1} - 2\alpha_n \beta \end{aligned} \tag{3.36c}$$

where

$$T^{n-1}_{j-1/2} = {}_n[(fv)^{n-1}_{j-1/2} - (u^2)^{n-1}_{j-1/2}] - h_j^{-1}[(b_1 v)^{n-1}_j - (b_1 v)^{n-1}_{j-1}]$$

$$\alpha_n = \frac{\bar{x}_{n-1/2}}{\bar{x}_n - \bar{x}_{n-1}} \qquad \beta = (p^*)^{n-1} - (p^*)^n$$

Equations (3.36) are imposed for $j = 1,2,\ldots, J$. The wall boundary conditions of equation (2.23b), with the new dependent variables defined in equation (3.34), yield, at $\bar{x} = \bar{x}_n$,

$$f^n_o = 0 \qquad u^n_o = 0 \tag{3.37a}$$

Similarly, the outer boundary conditions of equation (2.24) can be written as

$$(u^2)^n_J = (u^2)^{n-1}_J + 2\beta \tag{3.37b}$$

If $(f^{n-1}_j, u^{n-1}_j, v^{n-1}_j)$ and β^n are assumed known for $0 \le j \le J$, then equation (3.36), for $1 \le j \le J-1$ and the boundary conditions of equation (3.37), yield a nonlinear algebraic system of $3J+3$ equations in as many unknowns (f^n_j, u^n_j, v^n_j). The system can be easily solved by block elimination after linearization by Newton's method. Details of Newton's method and the block elimination method for the momentum equation, including the corresponding computer program program, are provided in [28].

To determine the value of $\partial\phi/\partial\beta$, in equation (3.31), it is necessary to know $\partial f/\partial\beta$ at $(\bar{x}_n, \eta_L)$. Thus, equation (3.36) is differentiated with respect to β and leads to the following linear difference equations, known as the variational equations for equation (3.36):

$$h_j^{-1}(G_j^n - G_{j-1}^n) = U_{j-1/2}^n \qquad (3.38a)$$

$$h_j^{-1}(U_j^n - U_{j-1}^n) = V_{j-1/2}^n \qquad (3.38b)$$

$$h_j^{-1}[(b_1)_j^n V_j^n - (b_1)_{j-1}^n V_{j-1}^n] - \alpha_n(u_j^n U_j^n + u_{j-1}^n U_{j-1}^n)$$
$$+ \left(\frac{1}{4} + \frac{\alpha}{2}\right)(f_j^n V_j^n + v_j^n G_j^n + f_{j-1}^n V_{j-1}^n + v_{j-1}^n G_{j-1}^n) \qquad (3.38c)$$
$$+ \frac{1}{2}\alpha_n\left[v_{j-1/2}^{n-1}(G_j^n + G_{j-1}^n) - f_{j-1/2}^{n-1}(V_j^n + V_{j-1}^n)\right] = -2\alpha_n$$

Similarly, the boundary conditions of equation (3.37) yield

$$G_o^n = 0 \qquad U_o^n = 0 \qquad U_J^n = 1/u_J^n \qquad (3.39)$$

In equations (3.38) and (3.39), the following notation has been introduced:

$$G \equiv \frac{\partial f}{\partial \beta} \qquad U \equiv \frac{\partial u}{\partial \beta} \qquad V \equiv \frac{\partial v}{\partial \beta} \qquad (3.40)$$

In common with the standard problem, equations (3.38) and (3.39) form a tridiagonal system, with 3x3 blocks, which is solved by the block elimination method referred to above and described, in detail, in reference 28.

3.3 Momentum Equation and the Mechul Method for Internal Flows

In contrast to the nonlinear eigenvalue approach, the Mechul method solves directly for β and eliminates the need for iteration. Thus the conservation equations, in transformed variables, again contain one unknown more than the number of equations. Mass continuity, in integral form, together with a knowledge of the duct geometry provides the required additional information and allows explicit solution of the equation, without iteration, and with pressure obtained from the solution. With the function p^* treated as unknown and with the help of the y-momentum equation $(-\partial p^*/\partial \bar{y} = 0)$ equation (2.18) can be written

$$f' = u \tag{3.41a}$$

$$u' = v \tag{3.41b}$$

$$(p^*)' = 0 \tag{3.41c}$$

$$(b_1 v)' + \frac{1}{2} fv = \bar{x}\left(\frac{dp^*}{d\bar{x}} + u\frac{\partial u}{\partial \bar{x}} - v\frac{\partial f}{\partial \bar{x}}\right) \tag{3.41d}$$

and the wall boundary conditions (2.23b) become:

$$\eta = 0 \qquad f = u = 0 \tag{3.42a}$$

Since as $y \to \delta$, $f \sim \eta$, an "edge" boundary condition for f at $\eta = \eta_\infty$ can be written with equation (2.28). Then the boundary conditions at the edge become

$$\eta = \eta_\infty \qquad f = u_e(\eta_\infty - \eta_L) + \sqrt{R_L}/\bar{x} \qquad u = u_e \tag{3.42b}$$

The difference equations for equation (3.41a,b,c) are similar to those given by equations (3.36a,b), and those for (3.41d) are similar to those of equation (3.36c), except that β is now variable; that is

$$h_j^{-1}(f_j^n - f_{j-1}^n) = u_{j-1/2}^n \tag{3.43a}$$

$$h_j^{-1}(u_j^n - u_{j-1}^n) = v_{j-1/2}^n \tag{3.43b}$$

$$h_j^{-1}(p_j^n - p_{j-1}^n) = 0 \tag{3.43c}$$

$$h_j^{-1}[(b_1)_j^n v_j^n - (b_1)_{j-1}^n v_{j-1}^n] + \left(\frac{1}{2} + \alpha_n\right)(fv)_{j-1/2}^n - \alpha_n\left[2p_{j-1/2}^n + (u^2)_{j-1/2}^n - v_{j-1/2}^{n-1} f_{j-1/2}^n + f_{j-1/2}^n v_{j-1/2}^{n-1}\right] = R_{j-1/2}^{n-1} \tag{3.43d}$$

Here

$$R_{j-1/2}^{n-1} = \alpha_n\left[(fv)_{j-1/2}^{n-1} - (u^2)_{j-1/2}^{n-1} - 2p_{j-1/2}^{n-1}\right] - h_j^{-1}\left[(b_1 v)_j^{n-1} - (b_1 v)_{j-1}^{n-1}\right] - \frac{1}{2}(fv)_{j-1/2}^{n-1}$$

Similarly the boundary conditions (3.42a,b) become

$$f_o^n = u_o^n = 0, \qquad u_J^n = u_e^n, \qquad f_J^n = u_J^n(\eta_\infty - \eta_L) + \sqrt{R_L}/\bar{x} \tag{3.44}$$

The solution of the system given by equations (3.43) and (3.44) is similar to that for the standard problem. This time there is a nonlinear algebraic system of $4J+4$ equations in as many unknowns $(f_j^n, u_j^n, v_j^n, p_j^n)$. Again the system can be solved with the block elimination method discussed earlier after linearization by Newton's method.

For flows with negative wall shear, it is necessary to make approximations to the governing equations to continue the calculations past the separation point. Here we use the approximation first suggested by Reyhner and Flügge-Lotz [32]. This approximation referred to as FLARE by Williams [24], neglects the $u(\partial u/\partial x)$ term in the region of negative u-velocity, $u < 0$. All inverse boundary-layer procedures, including the Mechul method described above, use this approximation for regions of separated flow. Once a solution has been obtained with this approximation, however, the assumption can be relaxed to allow solutions of the complete boundary-layer equations. For details, the reader is referred to [11].

3.4 Energy Equation for Internal Flows

The method used to obtain solutions to equation (2.19) is similar to that described in section 3.2 except that the iteration technique, necessitated by the presence of pressure gradient, is no longer required. Again, a new dependent variable $w(\bar{x},\eta)$ is defined, i.e.

$$g' = w \tag{3.45a}$$

and equation (2.19) rewritten as:

$$(b_2 w)' + \frac{1}{2} Pr\, fw = Pr\, \bar{x} \left(u \frac{\partial g}{\partial \bar{x}} - w \frac{\partial f}{\partial \bar{x}} \right) \tag{3.45b}$$

Equation (3.45a) is centered at $(x_n, \eta_{j-1/2})$ and equation (3.45b) at $(\bar{x}_{n-1/2}, \eta_{j-1/2})$ to obtain the finite-difference equations.

$$g_j^n - g_{j-1}^n - \frac{h_j}{2}(w_j + w_{j-1}) = 0 \tag{3.46a}$$

$$(\zeta_1)_j w_j + (\zeta_2)_j w_{j-1} + \zeta_3(g_j + g_{j-1}) = (r_1)_j \tag{3.46b}$$

Here

$$(\zeta_1)_j = \frac{(b_2)_j^n}{h_j} + Pr\left[\frac{1}{2} f_{j-1/2}^n + \alpha_n (f_{j-1/2}^n - f_{j-1/2}^{n-1})\right]$$

$$(\zeta_2)_j = -\frac{(b_2)_{j-1}^n}{h_j} - \frac{(b_2)_j^n}{h_j} + (\zeta_1)_j \tag{3.47}$$

$$(\zeta_3)_j = -2Pr\ \alpha_n u_{j-1/2}^{n-1/2}$$

$$(r_1)_j = -h_j^{-1}\left[(b_2)_j^{n-1} w_j^{n-1} - (b_2)_{j-1}^{n-1} w_{j-1}^{n-1}\right] - \frac{Pr}{2}(fw)_{j-1/2}^{n-1} - Pr\ \alpha_n\left[2u_{j-1/2}^{n-1/2}\ g_{j-1/2}^{n-1} + (f_{j-1/2}^n - f_{j-1/2}^{n-1}) w_{j-1/2}^{n-1}\right]$$

The solution of the linear system, subject to the general wall boundary conditions

$$\alpha_0 g_0^n + \alpha_1 w_0^n = \gamma_0 \tag{3.48a}$$

and to the general "edge" boundary conditions

$$\beta_0 g_J^n + \beta_1 w_J^n = \gamma_1 \tag{3.48b}$$

can be obtained by the same block elimination method used with the momentum equation.

The system of equations (3.46) and (3.47) has a block tridiagonal structure which is shown in matrix-vector form indicated below:

$$
\begin{array}{l}
 \\
\text{b.c. eq.(3.48a)} \\
\text{eq. (3.46a)} \\
\text{eq. (3.46b)} \\
 \\
 \\
\text{b.c. eq.(3.48b)}
\end{array}
\begin{array}{c}
\begin{array}{cccccc} g_0 & w_0 & g_j & w_j & g_J & w_J \end{array} \\
\left[\begin{array}{cccccc}
\alpha_0 & \alpha_1 & 0 & 0 & & \\
-1 & \frac{-h_1}{2} & 1 & \frac{-h_1}{2} & & \\
(\zeta_3)_j & (\zeta_2)_j & (\zeta_3)_j & (\zeta_1)_j & 0 & 0 \\
0 & 0 & -1 & \frac{-h_{j+1}}{2} & 1 & \frac{-h_{j+1}}{2} \\
 & & (\zeta_3)_J & (\zeta_2)_J & (\zeta_3)_J & (\zeta_1)_J \\
 & & 0 & 0 & \beta_0 & \beta_1
\end{array}\right]
\end{array}
\begin{array}{c}
 \\
 \\
 \\
\left[\begin{array}{c} g_0 \\ w_0 \end{array}\right] \\
\left[\begin{array}{c} g_j \\ w_j \end{array}\right] \\
\left[\begin{array}{c} g_J \\ w_J \end{array}\right]
\end{array}
=
\begin{array}{c}
 \\
 \\
 \\
\left[\begin{array}{c} (r_1)_0 \\ (r_2)_0 \end{array}\right] \\
\left[\begin{array}{c} (r_1)_j \\ (r_2)_j \end{array}\right] \\
\left[\begin{array}{c} (r_1)_J \\ (r_2)_J \end{array}\right]
\end{array}
\tag{3.49}
$$

This equation can also be written as in (3.25) and may be solved by the procedure described following equation (3.25).

3.5 Comments on the Solution Algorithm

The Box method allows nonuniform net spacings in the streamwise direction and across the boundary layer. The use of nonuniform net spacing across the layer is essential for turbulent flow calculations. This can be achieved by using a grid which has the property that the ratio of lengths of any two adjacent intervals is a constant; that is, $h_j = Kh_{j-1}$. The distance to the j-th line is given by the following formula:

$$\eta_j = h_1(K^j - 1)/(K - 1) \quad K > 1 \tag{3.50}$$

There are two parameters: h_1, the length of the first $\Delta\eta$ step, and K, the ratio of two successive steps. The total number of points J can be calculated from the expression,

$$J = \frac{\ln[1 + (K - 1)(\eta_\infty / h_1)]}{\ln K} \tag{3.51}$$

For further details, see Cebeci and Bradshaw [28].

4.0 RESULTS

The present results section has been prepared in six subsections. The first considers laminar internal flows and, in view of the greater importance of turbulent flow and the considerable attention previously devoted to this topic, is not extensive. It serves, however, to provide confidence in the abilities of the numerical method and to demonstrate its efficiency. The eddy-viscosity and turbulent Prandtl-number assumptions are described in subsection 4.2 and briefly compared with available alternatives. Turbulent internal-flow results, obtained with the assumptions of subsection 4.2 and with the numerical method of subsections 3.2 and 3.4 are presented in subsection 4.3 and compared with previous calculations and measurements. New internal-flow results are presented in subsection 4.4 to quantify the influence of Reynolds number on the Stanton number distribution for pipe flow, including regions of laminar, transition and turbulent flow. Separated flows are considered in subsections 4.5 and 4.6 where the Mechul approach of subsection 3.3 is applied to laminar and turbulent external flows, respectively. The internal-flow results are based on those of reference 8 and the separated-flow results of reference 9.

4.1 Laminar Internal Flow

It is difficult to find useful practical applications for results relating to the entrance region of a pipe flow, where the initial profile is presumed uniform. Nevertheless, a large number of computational investigations have been reported and a sample are referred to in table 1. Corresponding experiments have also been reported largely because of the interest stemming from transpiration viscometers of finite inlet length. In practice, the initial

profile depends upon the shape of the entrance to the tube and on the expansion ratio, as is witnessed by the experimental results referred to in table 1. It may be assumed that for a sharp-edged entrance normal pressure gradients and small regions of flow separation will exist and may invalidate the boundary-layer assumptions.

Nevertheless, and to provide a sample laminar-duct-flow calculation which may be compared with previous results, the laminar entrance-flow problem has been considered and solutions obtained. A sample of the results are reproduced by Cebeci and Bradshaw [28] and may be supplemented by figure 6 which presents the calculated distribution of nondimensional pressure drop from the tube entrance, where uniform velocity has been assumed, to the downstream parabolic profile region. The solutions of Langhaar [33] and Campbell and Slattery [34] are also shown together with the Poiseuille flow asymptote. Experimental data have also been reported, for example by Pfenninger [35], Shapiro, Siegel and Kline [36] and by Whitelaw [37] and, as can be seen, for example, from the

Table 1. Kinetic energy correction factor h defined by $\frac{p - p_o}{(1/2)\, u_o^2} = 64x^{**} + 2h$

Calculated	
Present Investigation	1.123
Langhaar [33]	1.14
Campbell and Slattery [34]	1.09
Measured	
Schiller [38]	1.058 – 1.225
Rieman [39]	1.110 – 1.134
Swindells et al [40]	1.12 – 1.17

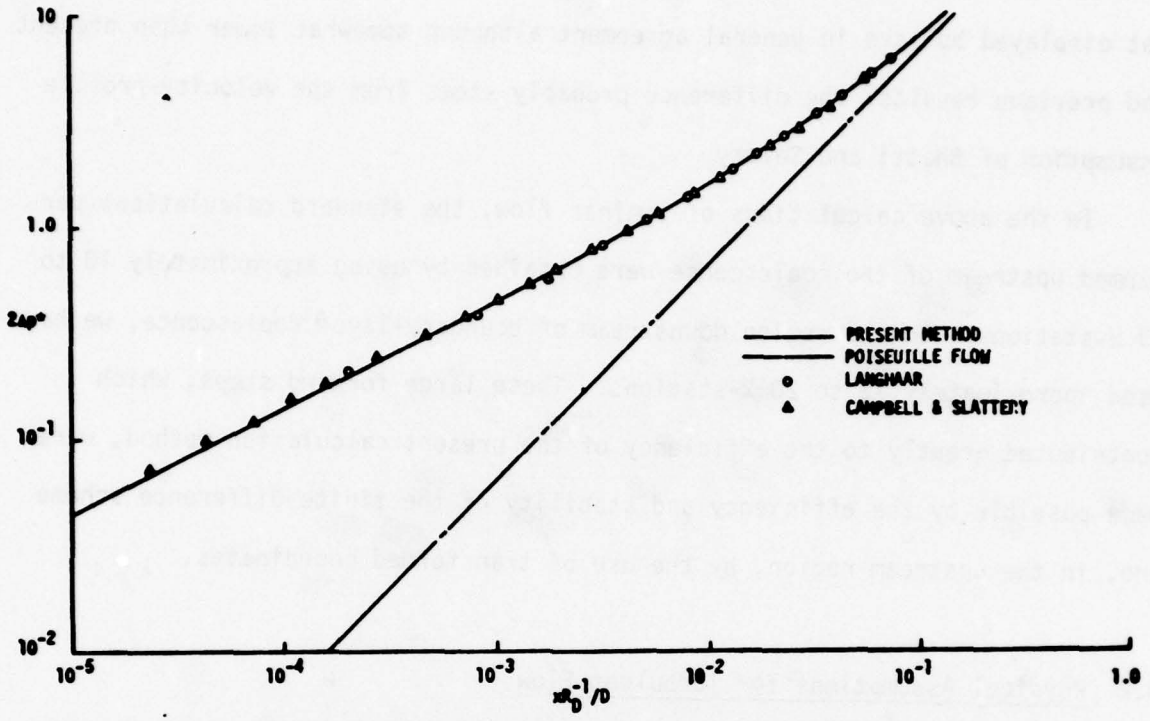

Figure 6. Pressure drop for laminar flow in a circular pipe.

paper of Campbell and Slattery, are subject to scatter but tend to support the present results. Since viscometry is a likely application of results to the entrance-length problem, table 1 presents calculated and measured values of the so-called "kinetic-energy correction factor."

An example of heat-transfer calculations, for flow in a two-dimensional plane channel with developing momentum and thermal boundary layers with constant heat flux are presented in figure 7. The results may be compared with the previous calculations of Siegel and Sparrow [41] and Naito [42], which have been represented by a number of discrete points taken from the plotted results, and are in excellent agreement except at the lowest values of the Prandtl number. The more recent results of Bhatti and Savery [43], which

also made use of the Karman-Pohlhausen method to solve the energy equation, are not displayed but are in general agreement although somewhat lower than present and previous results; the difference probably stems from the velocity-profile assumption of Bhatti and Savery.

In the above calculations of laminar flow, the standard calculations performed upstream of the coalescence were obtained by using approximately 10 to 15 x-stations. In the region downstream of boundary-layer coalescence, we have used approximately 15 to 20 x-stations. These large forward steps, which contributed greatly to the efficiency of the present calculation method, were made possible by the efficiency and stability of the finite-difference scheme and, in the upstream region, by the use of transformed coordinates.

4.2 Physical Assumptions for Turbulent Flow

For turbulent flows in ducts, there are essentially three distinct regions. Near the entrance, the shear layers develop in the region close to the solid

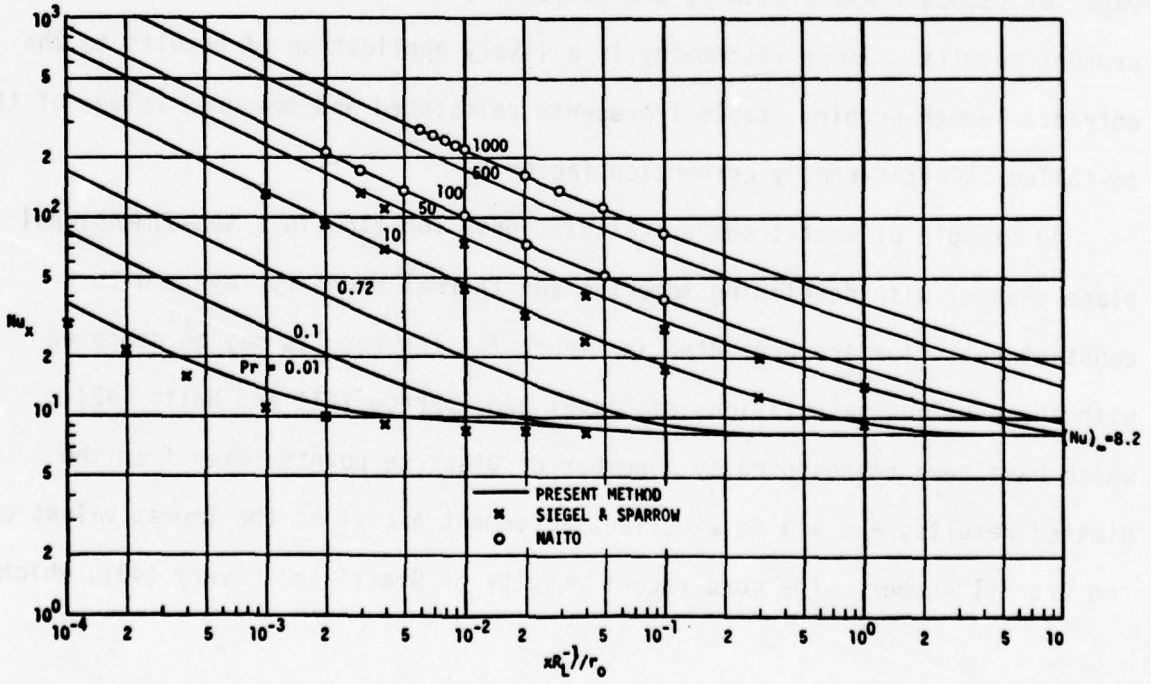

Figure 7. Local Nusselt number distributions for laminar flow in a plane channel with constant wall heat flux.

wall and the core velocity increases continuously due to the growth in displacement thickness. The flow in this region, which may be called the displacement-interaction region [43], is physically no more than the boundary-layer flow in a mild favorable pressure gradient.

As the flow moves downstream, the shear layers grow and finally meet on the centerline. The shear-layer interaction increases in strength until a steady state of mutual eddy intrusion and fine-scale mixing is achieved, where the flow is fully developed.

The eddy-viscosity concept is used here to model the Reynolds shear stress, $-\rho\overline{u'v'}$ and, in the displacement interaction region, the formulation is that of reference 18:

Inner layer

$$\varepsilon_i = \{\kappa y[1 - \exp(-y/A)]\}^2 \left|\frac{\partial u}{\partial y}\right| \qquad \varepsilon_i \leq \varepsilon_o \tag{4.1a}$$

Outer layer

$$\varepsilon_o = 0.0168 \left|\int_0^\infty (u_e - u)dy\right| \tag{4.1b}$$

Here

$$\kappa = 0.40, \qquad A = 26\nu/u_\tau, \qquad u_\tau = \sqrt{\tau_w/\rho} \tag{4.2}$$

In the fully developed region, we use the well-known mixing-length formula of Nikuradse and express the eddy viscosity for the entire layer by

$$\varepsilon = \left\{\ell[1 - \exp(-y/A)]\right\}^2 \left|\frac{\partial u}{\partial y}\right| \tag{4.3}$$

where

$$\ell = r_o[0.14 - 0.08(1 - r/r_o)^2 - 0.06(1 - r/r_o)^4] \qquad (4.4)$$

To use equation (4.4) for two-dimensional duct flows, we simply set $r_o = h$ to get

$$1 - \frac{r}{r_o} = y/h$$

For the region between the displacement interaction and fully developed regions, the eddy-viscosity formula is given by the following expression that combines equation (4.1) and (4.4)

$$\varepsilon = \varepsilon_I + (\varepsilon_F - \varepsilon_I)\left\{1 - \exp\left[-\frac{(x - x_o)}{\lambda r_o}\right]\right\} \qquad (4.5)$$

with ε_I denoting the formula given by equation (4.1), ε_F the formula by equation (4.3), and with λ denoting an empirical constant.

In cases where the location of the onset of transition is known, the flow may be determined through the transition region and into the fully turbulent region by multiplying the expressions for ε by an intermittency factor γ_{tr}, defined by

$$\gamma_{tr} = 1 - \exp\left[-\frac{1}{1200} R_{x_{tr}}^{0.66}\left(\frac{x}{x_{tr}} - 1\right)^2\right] \qquad (4.6)$$

For calculations requiring solutions of the energy equation for turbulent flows, a turbulent Prandtl number may be specified. Here we use the formula described in [1]. According to that formula, the turbulent Prandtl number Pr_t, is computed from

$$Pr_t = \frac{0.40[1 - \exp(-y/A)]}{0.44[1 - \exp(-y/B)]} \qquad (4.7)$$

with

$$B = B^+ \nu/u_\tau, \qquad B^+ = \frac{1}{(Pr)^{1/2}} \sum_{1}^{5} C_i (\log Pr)^{i-1} \tag{4.8}$$

$$C_1 = 34.96, \quad C_2 = 28.79, \quad C_3 = 33.95, \quad C_4 = 6.33 \quad \text{and} \quad C_5 = -1.186$$

4.3 Turbulent Internal Flow

For the convenience of the reader, a sample of the results obtained for turbulent flow are presented in the following paragraphs. The capabilities of the turbulence model and its relationship to alternatives are discussed after the results and the comparisons with measurements have been introduced.

Most of the turbulent flows considered here relate to plane channels, but to preserve symmetry with section 4.1, it is useful to start with pipe-flow results. The measurements of Barbin and Jones [45] provide an example of a developing pipe flow which, in the near fully-developed condition, accords with the classical measurements of Laufer [46]. It should be emphasized that the "fully-developed" conditions are achieved asymptotically and, at their diameter Reynolds number of 3.88×10^5, Barbin and Jones concluded that it had not been achieved at 40.5 diameters. The pressure-drop results of figure 8, which are perhaps the least sensitive check, would suggest that the flow was very close to the asymptote. The computed nondimensional centerline velocity distribution is also shown on figure 8a and, like the pressure-drop data, is in close accord with measurements although in the region where the boundary layers fill the pipe, they show a more rapid change in shape than the

measurements. This slight discrepancy between calculations and measurements can be attributed to the form of the eddy-viscosity hypothesis and is not reflected in the profiles of figure 8b. The calculations began with the measured profile at x/D of 1.5.

The turbulent flow in two-dimensional channels has been investigated by many authors and, together with the pipe-flow investigations, has added a great deal to an understanding of turbulent flows in general and near-wall flows in particular. The contributions of Laufer [47] and Comte-Bellot [48] are perhaps best known although the more recent paper by Hussain and Reynolds [49] uses the largest aspect ratio of 18:1; this is not to say that the resulting flow is necessarily the most two-dimensional. In addition, isothermal

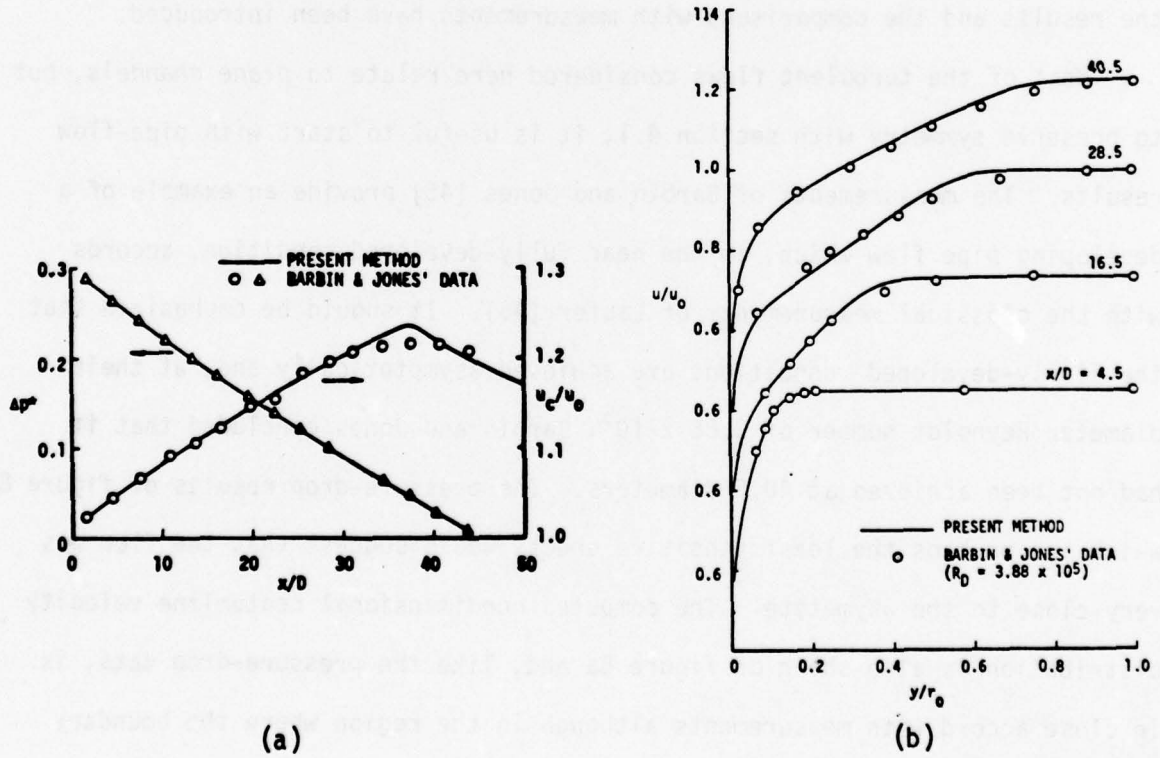

Figure 8. Comparison of present calculations with Barbin and Jones' pipe-flow measurements. (a) Centerline velocity and pressure drop. (b) Velocity profiles.

two-dimensional plane channel results have been reported, for example by Clark [50], Byrne, Hatton and Marriott [51] and Dean [52]. The sample of calculated results shown on figures 9 to 11 has been presented to display a range of properties as well as to allow comparison with the results of three experiments.

Figure 9 compares calculated velocity profiles with the measurements of Comte-Bellot. The calculations began with the measured profile at x/D of 20 and, as can be seen, are in very close accord with the measurements. Distributions of displacement and momentum thickness, corresponding to the experiment of Byrne et al. [51] are presented in figure 10, and it is

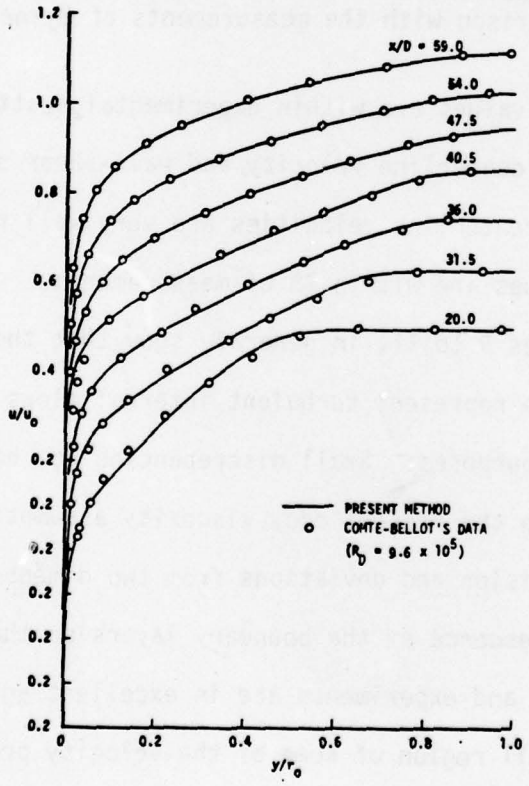

Figure 9. Comparison of calculated velocity profiles with the measurements of Comte-Bellot.

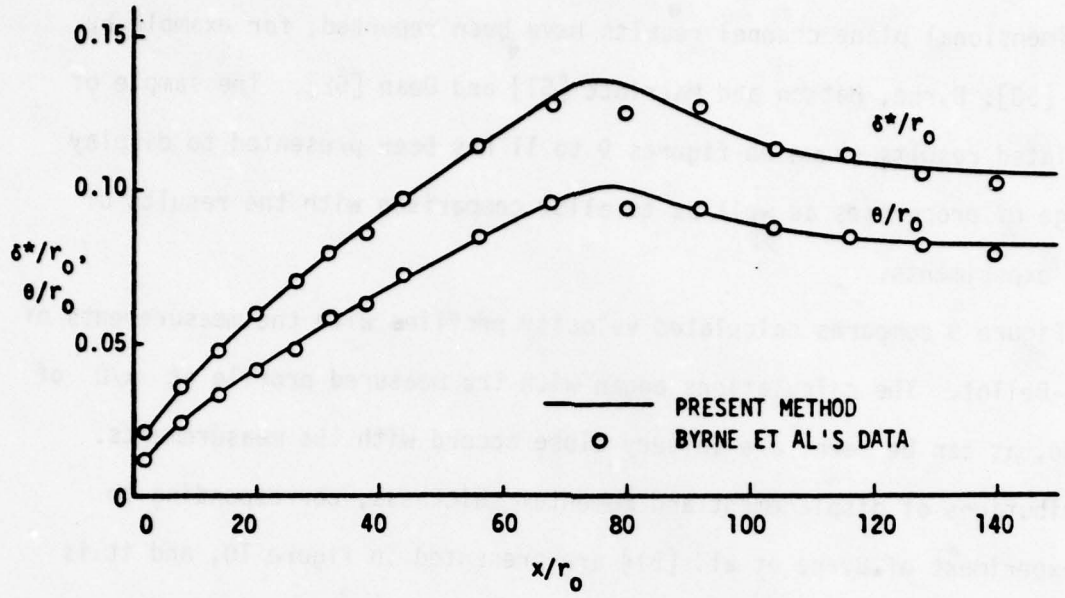

Figure 10. Computed displacement and momentum thickness distributions in a plane channel; comparison with the measurements of Byrne et al.

clear that the calculated values are within experimental scatter. Dean's data [50] for velocity profile centerline velocity and wall-shear stress are presented in figure 11; the centerline velocities are very well represented and the wall-shear stress values are within 7% of measurements.

The results of figures 9 to 11, in general, show that the present calculation method is able to represent turbulent internal flows with adequate accuracy for engineering purposes. Small discrepancies do, however, exist and are partly attributable to the present eddy-viscosity assumption and partly due to measurement imprecision and deviations from two dimensionality. In the flow upstream of the coalescence of the boundary layers on the two sides of the channel, the calculations and experiments are in excellent agreement apart, perhaps, from the near-wall region of some of the velocity profiles of Comte-Bellot. In this region, the inner-layer expression for eddy viscosity

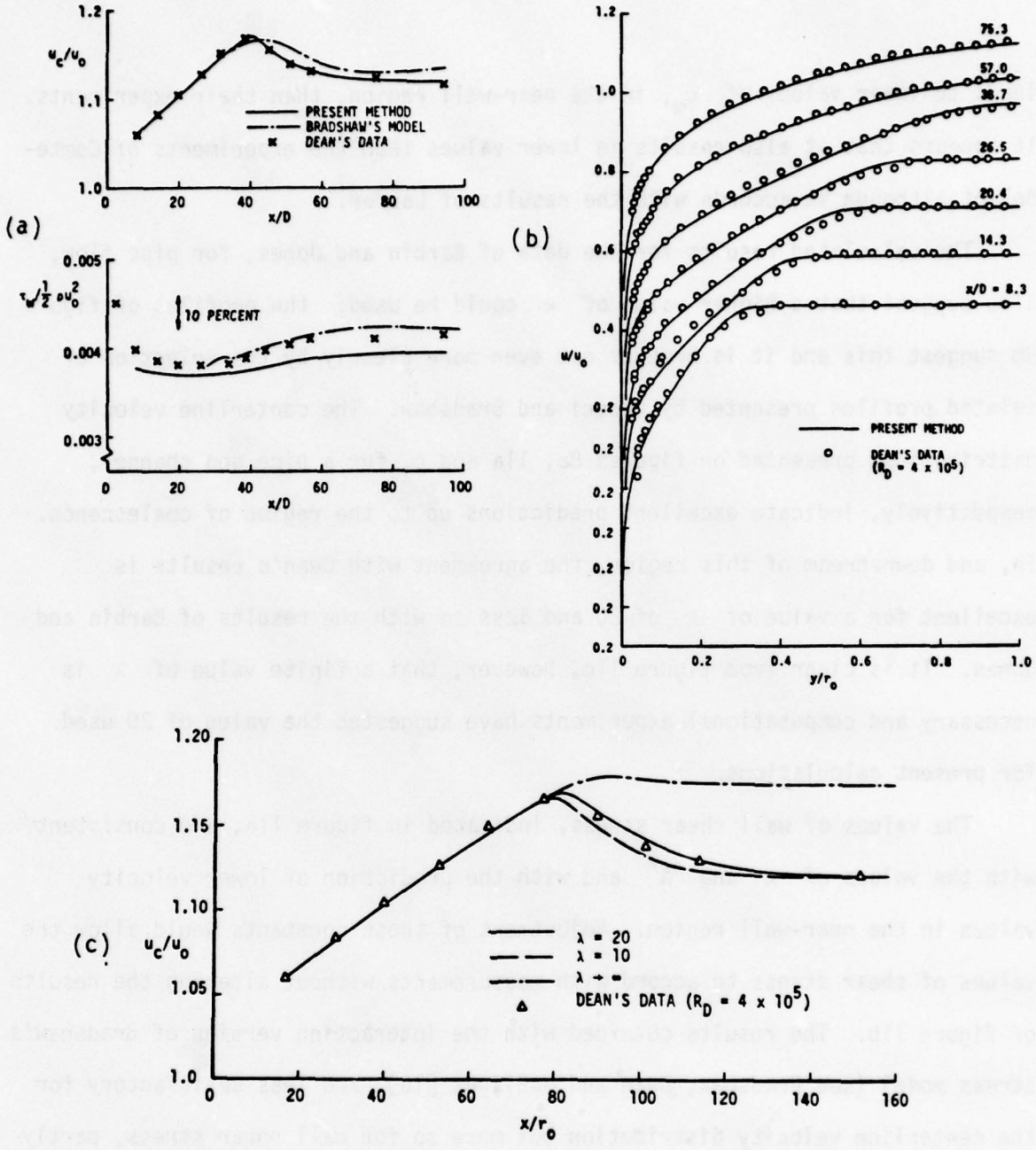

Figure 11. Comparison of present calculations with Dean's plane channel-flow measurements. (a) Centerline velocity and shear stress. (b) Velocity profiles. (c) Centerline velocity with different values of the parameter λ.

dominates the calculated results which are strongly dependent on the value of the von Karman constant, κ. The value of κ used in this region was 0.4. As pointed out by Hussain and Reynolds, however, this value with an A^+ of 26

leads to lower values of ε_m, in the near-wall region, than their experiments. It appears that it also results in lower values than the experiments of Comte-Bellot although it accords with the results of Laufer.

The calculated results for the data of Barbin and Jones, for pipe flow, also suggest that a higher value of κ could be used: the profiles of figure 8b suggest this and it is brought out even more clearly by the selection of related profiles presented by Cebeci and Bradshaw. The centerline velocity distributions presented on figures 8a, 11a and c, for a pipe and channel, respectively, indicate excellent predictions up to the region of coalescence. In, and downstream of this region, the agreement with Dean's results is excellent for a value of λ of 20 and less so with the results of Barbin and Jones. It is clear from figure 11c, however, that a finite value of λ is necessary and computational experiments have suggested the value of 20 used for present calculations.

The values of wall shear stress, indicated in figure 11a, are consistent with the values of κ and A^+ and with the prediction of lower velocity values in the near-wall region. Adjustment of these constants would allow the values of shear stress to accord with measurements without altering the results of figure 11b. The results obtained with the interacting version of Bradshaw's stress model (see Bradshaw, Dean and McEligot [16]) are less satisfactory for the centerline velocity distribution but more so for wall shear stress, partly due to the use of 0.41 as the von Karman constant.

Both Na and Habib [13] and Stephenson [53] have obtained calculated distributions of Nusselt number as a function of Reynolds number for fully-developed turbulent flows in round pipes and for a Prandtl number. As indicated by Habib and Na [14], the results are essentially independent of the temperature boundary condition and this is supported by the present results which are shown on figure 12 for a laminar Prandtl number of 0.72. As expected, the resulting

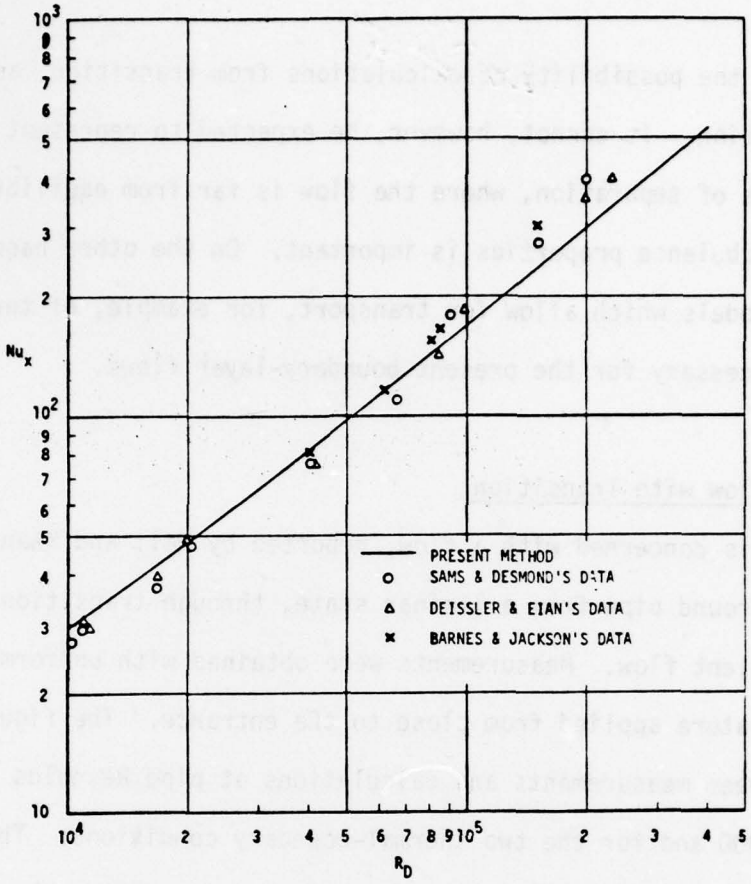

Figure 12. Computed local Nusselt number for fully-developed pipe flow with constant wall heat flux and constant wall temperature; comparison with experimental data. For references see [13].

curve is very similar to those of Na and Habib. For a bulk Reynolds number of 3.88×10^5, the value of Stanton number is 1.85×10^{-3} which may be compared with Stephanson's value of 2.0×10^{-3}. (The corresponding results for fully-developed, two-dimensional, plane channel flow with a bulk Reynolds number of 1.92×10^5 are 2.19×10^{-3} and 2.47×10^{-3}.)

The use of the present eddy-viscosity and turbulent Prandtl number formulations is clearly successful in that they allow the flows examined in this section to be very well represented. It is possible to make use of simple or more complicated approaches. The present eddy viscosity is probably the simplest which can be used to represent external and internal boundary layers

and still allow the possibility of calculations from transition, as demonstrated in the next section. It cannot, however, be expected to represent flows, such as large regions of separation, where the flow is far from equilibrium and transport of turbulence properties is important. On the other hand, the use of turbulence models which allow for transport, for example, of turbulence energy are unnecessary for the present boundary-layer flows.

4.4 Internal Flow with Transition

Figure 13 is concerned with a flow, reported by Hall and Khan [54], which developed in a round pipe from a laminar state, through transition to fully-developed turbulent flow. Measurements were obtained with uniform wall heat flux and temperature applied from close to the entrance. The figure allows comparison between measurements and calculations at pipe Reynolds numbers of 31,100 and 33,000 and for the two thermal-boundary conditions. The flow was assumed to undergo transition at $x = 4D$ where the Stanton number is minimum as shown in the experimental data. As can be seen, the agreement is good and the influence of the thermal boundary condition much greater in the region of transition than in the laminar and turbulent regions. The results of Hall and

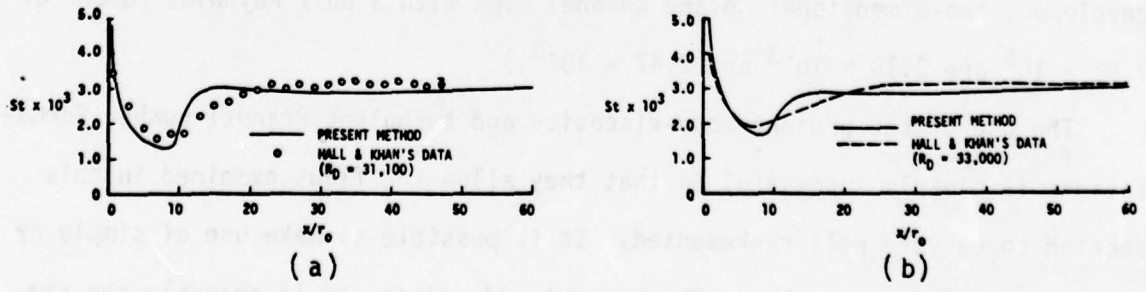

Figure 13. Computed local Stanton number in developing pipe flow; comparison with measurements of Hall and Khan for: (a) Constant heat flux. (b) Constant wall temperature.

Khan show that the influence of the thermal boundary condition diminishes with increasing Reynolds number and present calculations support this finding. Thus, the uniform wall heat-flux results of figure 14 accord with uniform wall-temperature results for values of R_D greater than 4×10^4 to better than 5% of the local value. The results of figure 14 were obtained with the assumption that the transition occurred at a value of momentum-thickness Reynolds number of 320.

4.5 Laminar Separated Flows

For laminar flows with separation, four separate external flows, which allow the displacement thickness distribution to be specified, have been considered. These include the laminar separated flows of Williams [25],

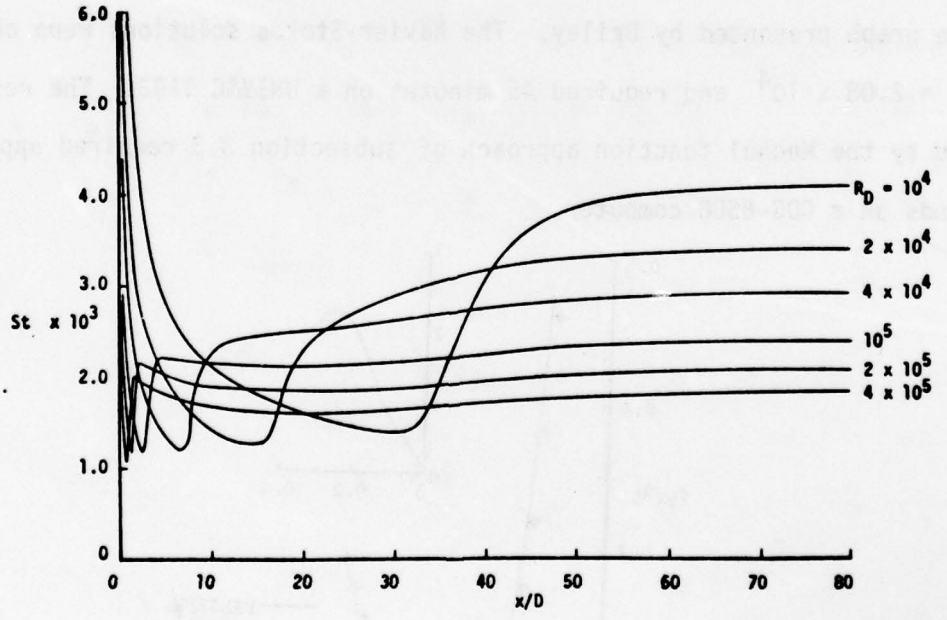

Figure 14. Local Stanton number distributions in developing pipe flow as a function of Reynolds number (Pr = 0.72 and $R_{\theta tr}$ = 320).

Carter [22] and Briley [26]. In the last case, the freestream boundary condition corresponded to a linearly decreasing external velocity distribution followed by a constant velocity and resulted in separation and reattachment. Figure 15 allows a comparison of values of local skin-friction coefficient $c_f \sqrt{R_L}$ calculated with the present method with those obtained by Briley from the steady, two-dimensional form of the Navier-Stokes equations. Here c_f is defined by

$$c_f = \frac{\tau_w}{1/2\ \rho u_0^2} = \frac{2f''(0)}{\sqrt{R_L}} \tag{4.9}$$

and $c_f\sqrt{R_L}$ represents $2f''(0)$. These calculations were made from the displacement thickness distribution (see figure 15) deduced from the Navier-Stokes solutions. In general, the agreement is very good and the small discrepancy may be associated with the difficulty of reading the input $\delta^*(x)$ distribution from the graph presented by Briley. The Navier-Stokes solutions were obtained for $R_L = 2.08 \times 10^4$ and required 45 minutes on a UNIVAC 1108. The results obtained by the Mechul function approach of subsection 3.3 required approximately 10 seconds on a CDC-6600 computer.

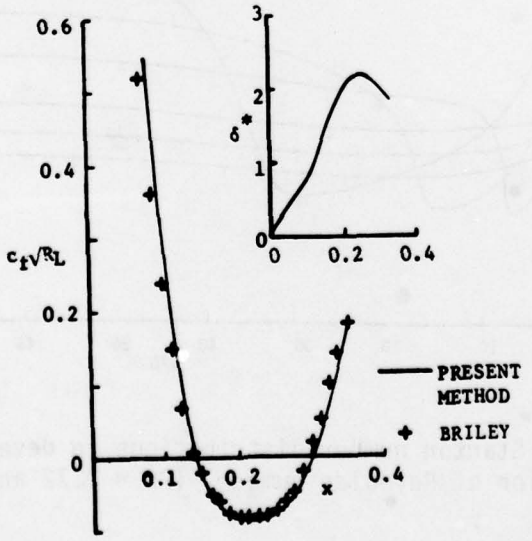

Figure 15. Calculated local skin-friction coefficient distribution for separating and reattaching flow computed by Briley [26].

We next consider the two laminar flows with separation and reattachment computed by Carter [22]. These flows have displacement-thickness distributions $\delta^*(x)$ given by

$$\bar{\delta}^*(x) \equiv \begin{cases} 1.7208\sqrt{x} & 1.0 \le x \le x_1 \\ a_1 + a_2(x - x_1) + a_3(x - x_1)^2 + a_4(x - x_1)^3 & x_1 \le x \le x_2 \\ \bar{a}_1 + \bar{a}_3(x - x_2)^2 + \bar{a}_4(x - x_2)^3 & x_2 \le x \le x_3 \end{cases} \qquad (4.10)$$

with

$$a_1 = 1.7208\ \sqrt{x_1}$$

$$a_2 = (0.5)(1.7208)/\sqrt{x_1}$$

$$a_3 = (0.5/\Delta_1)[6/\Delta_1(\delta^*_{max} - a_1) - 4a_2]$$

$$a_4 = 2/\Delta_1^3\ [\Delta_1/2a_2 - (\delta^*_{max} - a_1)]$$

$$\bar{a}_1 = \delta^*_{max}$$

$$\bar{a}_3 = -1/\Delta_2^2[3(\delta^*_{max} - \delta^*_3) + \Delta_2\delta^{*\prime}_3]$$

$$\bar{a}_4 = 1/\Delta_2^3\ [2(\delta^*_{max} - \delta^*_3) + \Delta_2\delta^{*\prime}_3]$$

$\Delta_1 = x_2 - x_1$, $\Delta_2 = x_3 - x_2$, $x_1 = 1.065$, $x_2 = 1.35$, $x_3 = 1.884$

The first flow, referred to as Case A, has $\delta^*_{max} = 5.6$, and the second flow referred to as Case B, has $\delta^*_{max} = 8.6$. The two displacement thickness distributions are shown in figures 16 and 17.

Comparison of present results with those of Carter [22] is shown in figures 16, 17, and 18. The present calculations were started at $x = 0$ by solving the governing equations in transformed variables for the standard problem and then at $x = 1$ the Mechul-function method of subsection 3.3 was used to solve the inverse problem with the equations expressed in physical variables.

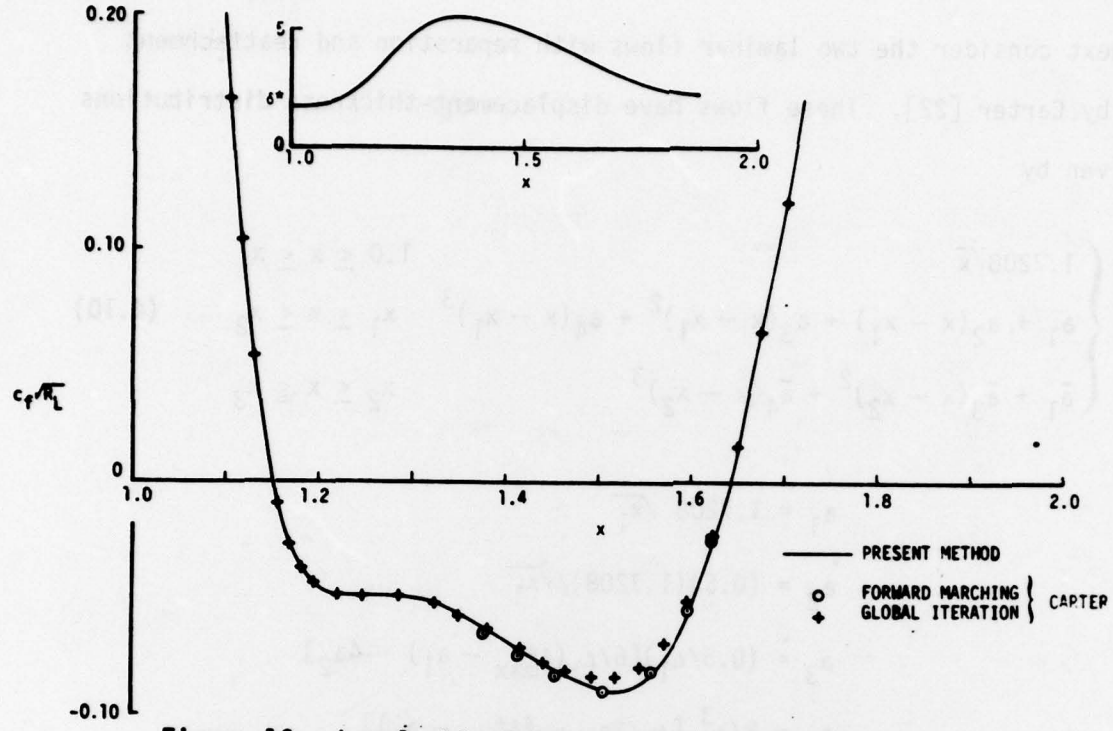

Figure 16. Local skin-friction distribution for Case A.

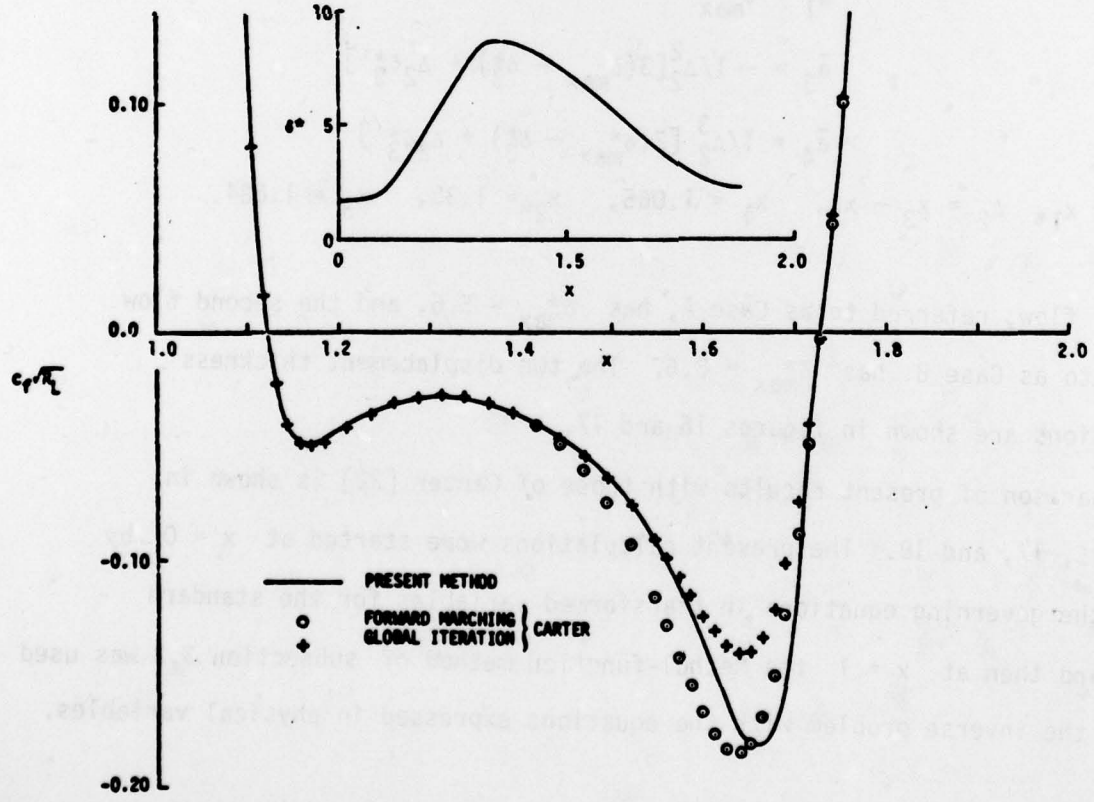

Figure 17. Local skin-friction distribution for Case B.

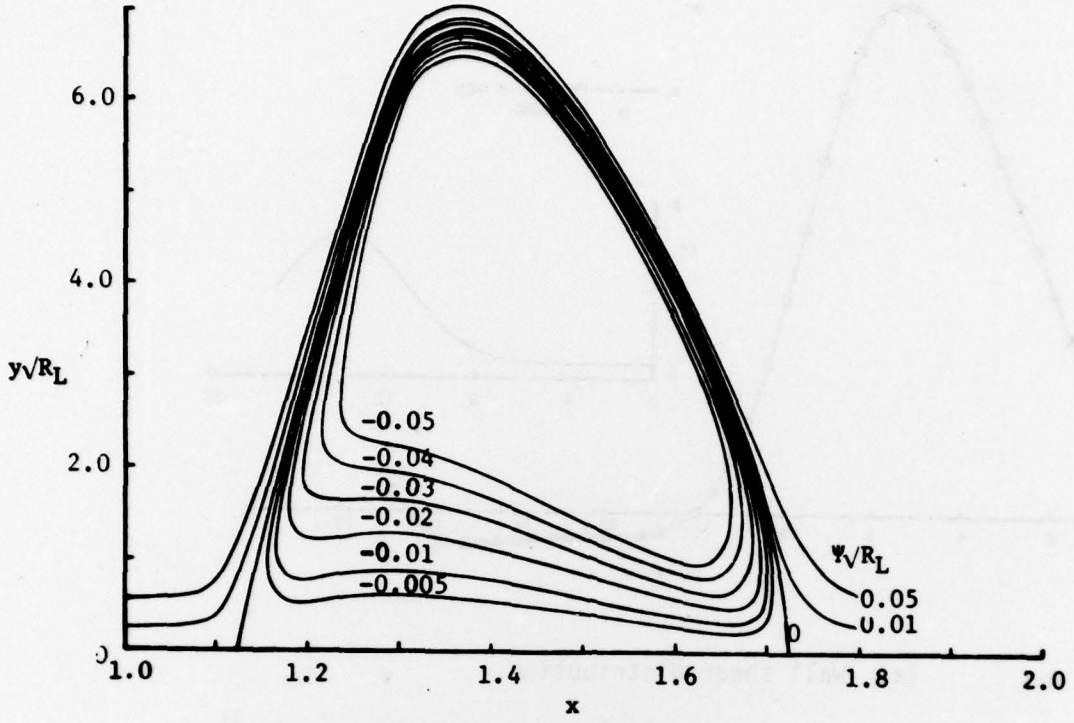

Figure 18. Streamline pattern in separation bubble for Case B.

As can be seen, the present results agree well with those of Carter which made use of the Reyhner and Flügge-Lotz approximations. Our skin-friction results are in better agreement with Carter's results. His Reyhner and Flügge-Lotz approximation was slightly different from that considered here and may account for the disagreement with the present results. The computer time associated with the results was again of the order of 10s on a CDC 6600. At almost all x-stations the convergence rate was quadratic and required only two or three iterations, including regions of separated flow.

Figure 19 shows the results for another laminar flow, with prescribed displacement thickness distribution, previously computed by Williams [25]. The δ^*-distribution is given by

$$\delta^* = 0.6479\{1 + 9\ \exp[-0.0625(x - 14)^2]\}$$

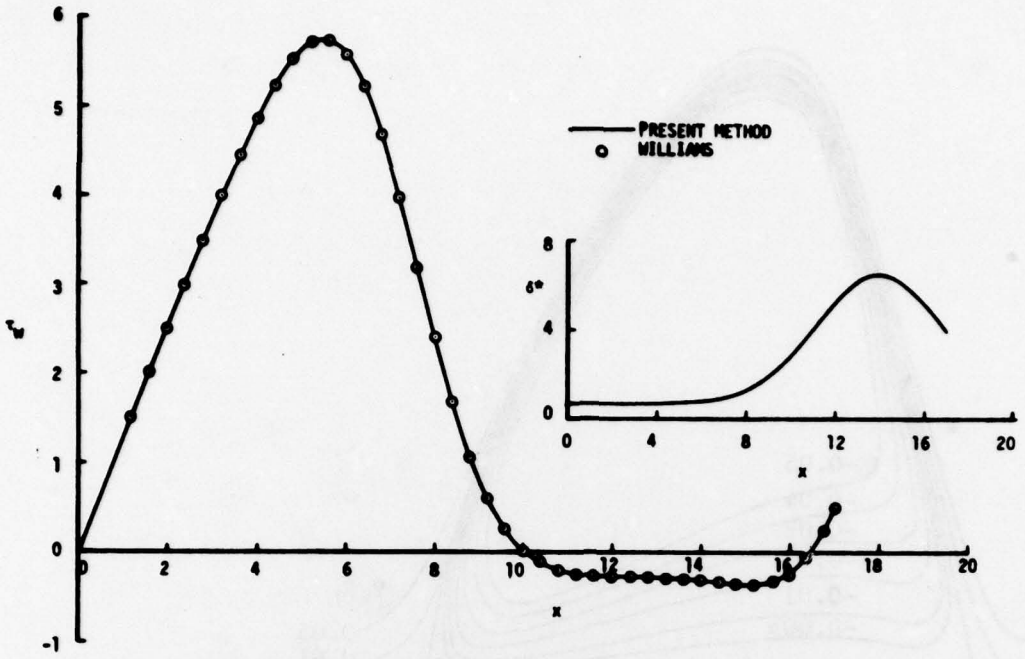

(a) Wall shear distribution.

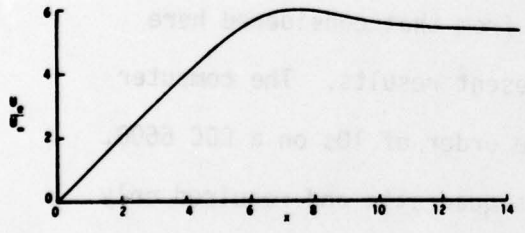

(b) External velocity distribution.

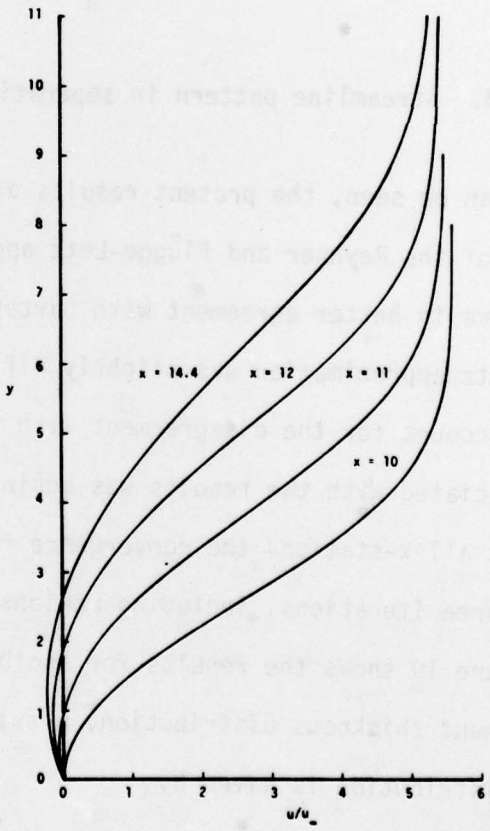

(c) Velocity profiles near and in the reverse flow region

Figure 19. Comparison of calculated results for the separated flow for which displacement-thickness distribution is given by equation (4.10).

In this case the flow starts at the stagnation-point and separates at approximately $x = 10$. Both calculations were made by the Reyhner and Flügge-Lotz approximation. As in the previous cases, the solutions converged quadratically requiring only two or three iterations, including regions of separated flow.

4.6 Turbulent Separated Flows

Two separate turbulent flows have been considered. These flows did not have flow separation and were computed with the eigenvalue and the Mechul-function methods to check the predictions of both methods for attaching flows. The two sets of results were identical. The application of the method for turbulent flows with separation is currently under examination.

The two attached turbulent flows were those measured by Schubauer and Spangenberg (see reference 27) and labeled as 4400 and 4800 at the 1968 Stanford Conference. Flow 4400 has a strong adverse pressure gradient and flow 4800 has a mild adverse pressure gradient. Figures 20 and 21 present the results for these two flows. The calculations were made first by using the standard procedure: in this case the external velocity distribution was specified and the boundary-layer parameters were computed. Next, the calculations were made with both of the inverse procedures: the measured displacement thickness distribution was specified and the external velocity distribution computed along with other boundary-layer parameters. As the results show, the agreement with experiment is very good; the difference between calculated and experimental velocity distributions is small, and the boundary-layer parameters computed by standard and inverse procedures agree with each other.

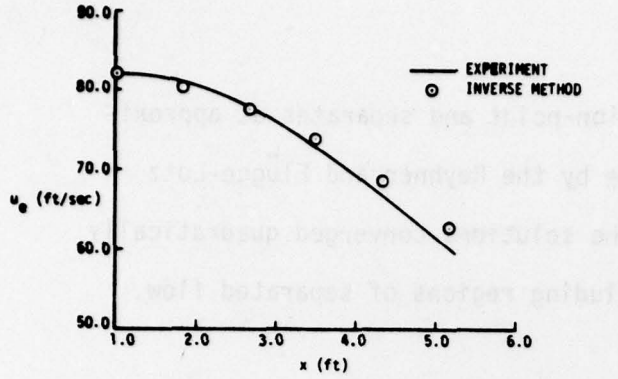

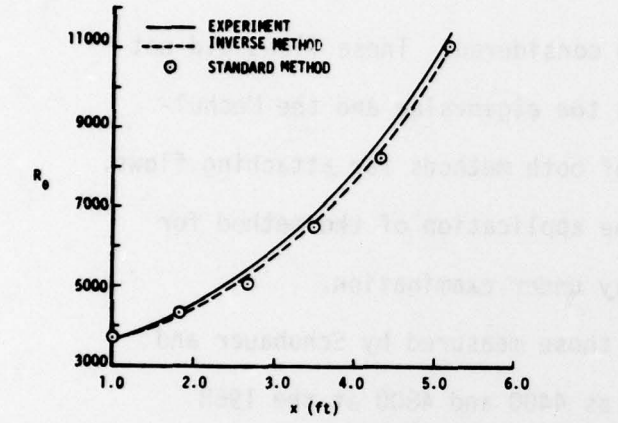

Figure 20. Results for flow 4400. (Inverse results were obtained by using both the nonlinear eigenvalue method and the Mechul-function method and are identical.)

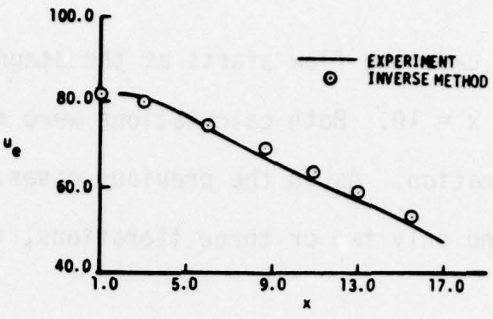

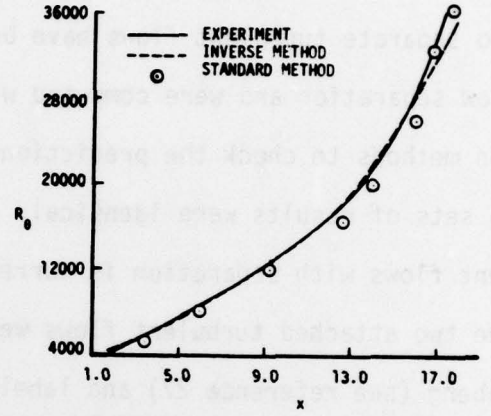

Figure 21. Results for flow 4800. (Inverse results were obtained by using both the nonlinear eigenvalue method and the Mechul-function method and are identical.)

5.0 CONCLUDING REMARKS

The results of the previous sections allow an evaluation of the calculation procedure in terms of the finite-difference method and the physical assumptions. Relevant comments have been included in section 4 and are summarized here.

Comparison of computer run times for internal-flow calculations with those of alternative numerical methods shows that the present formulation is advantageous for the boundary-layer problems which it is intended to solve. The reduction of the second-order equations to first-order, the introduction of transformed coordinates, and the use of the "Box" method of finite-differencing ensures that the efficiency is coupled with second-order accuracy. A typical computation time for a case using 41 nodes across the duct, and 35 axial stations down the duct was less than 2 seconds on an IBM 370/175. The chosen turbulence model is near optimum for the range of flow problems considered and has been shown to perform well, see for example, Cebeci and Smith [1] and Cebeci and Bradshaw [28], for a much wider range of boundary-layer problems including two-dimensional and three-dimensional external flows.

The separated flow results show that the present numerical scheme, with the Reyhner and Flügge-Lotz approximation [32] can be used to represent small regions of separated flow. The use of boundary-layer equations to represent separated flows presumes that the normal pressure gradient and longitudinal diffusion are small and the range of successful applicability remains to be determined. Nevertheless, it has been shown that the more efficient and accurate solution of boundary-layer equations will compensate for the approximations over a range of flows with small regions of recirculation. The more expensive solution of the elliptic equations, including the normal pressure-gradient and longitudinal-diffusion effects, becomes increasingly so as the number of grid

points is increased to make a finite-difference solution converge to the solution of the equations, see for example reference 10.

The following more important conclusions may be extracted from the present study:

1. The present numerical scheme allows the solution of boundary-layer equations, for a wide range of boundary conditions, with efficiency and accuracy. There are no significant difficulties in applying it to internal-flow problems.
2. The present eddy-viscosity and turbulent Prandtl number formulations, previously used in a wide range of external boundary-layer flows, has been shown to be equally satisfactory for a range of internal-flow problems.
3. The internal-flow problems considered include incompressible, two-dimensional laminar and turbulent pipe and plane-channel without and with heat transfer. Provided the location of the onset of transition is known, flow problems of this type including compressible flows can readily be solved with the present method.
4. The nonlinear eigenvalue method used to solve the internal-flow problems can be replaced by the Mechul-function method which can also be used to solve separated-flow problems. The present calculation demonstrate that the Mechul-function method, with a Reyhner and Flügge-Lotz approximation, conveniently leads to results which are in close agreement with previous calculations based on solution to the Navier-Stokes equations. Since the present procedure is considerably less expensive than solutions of the Navier-Stokes equations, the range of applicability should be established.

6.0 REFERENCES

1. Cebeci, T. and Smith, A.M.O. 1974. Analysis of Turbulent Boundary Layers. Academic Press.
2. Keller, H.B. 1970. A new finite-difference scheme for parabolic problems, in Numerical Solution of Partial-Differential Equations, ed. by J. Bramble, Vol. 2, Academic Press.
3. Cebeci, T. 1970. Calculation of laminar and turbulent boundary layers for two-dimensional time-dependent flows. NASA CR-2820.
4. Cebeci, T., Kaups, K. and Ramsey, J.A. 1977. A general method for calculating three-dimensional laminar and turbulent boundary layers on arbitrary wings. NASA CR-2777.
5. Cebeci, T. and Keller, H.B. 1977. Stability calculations for a rotating disk. AGARD Fluid Dynamics Panel Symposium on Laminar-Turbulent Transition, CPP 224, Copenhagen.
6. Keller, H.B. and Cebeci, T. 1972. An inverse problem in boundary-layer flows: Numerical determination of pressure gradient for a given wall shear. J. Comp. Phys., 10:151-161.
7. Cebeci, T. and Keller, H.B. 1974. Flows in ducts by boundary-layer theory. Proceedings of Fifth Australasian Conf. on Hydraulics and Fluid Mech., University of Canterbury, Christchurch.
8. Cebeci, T. and Chang, K.C. 1978. A general method for calculating momentum and heat transfer in laminar and turbulent duct flows. To be published in Int. J. Numerical Heat Transfer.
9. Cebeci, T. 1976. Separated flows and their representation by boundary-layer equations. Report ONR-CR215-234-2. Mech. Engg. Dept., California State University at Long Beach.

10. Cebeci, T., Khalil, E.E. and Whitelaw, J.H. 1977. Calculation of separated boundary-layer flows. Imperial College, Mech. Engg. Dept. Report FS/77/29.

11. Cebeci, T., Keller, H.B. and Williams, P.G. 1978. Separating boundary-layer flow calculations. To be published.

12. Tien, C. and Pawelek, R.A. 19 . Laminar flow heat transfer in the entrance region of circular tubes. Appl. Sci. Res., 13:317-331.

13. Na, T.Y. and Habib, I.S. 1973. Heat transfer in turbulent pipe flow based on a new mixing length model. App. Sci. Res., 28:302-314.

14. Habib, I.S. and Na, T.Y. 1974. Prediction of heat transfer in turbulent pipe flow with constant wall temperature. J. Heat Trans., 96:253-254.

15. Nelson, R.M. and Pletcher, R.H. 1974. An explicit scheme for the calculation of confined turbulent flows with heat transfer. Proc. 24th Heat Transfer and Fluid Mechanics Institute.

16. Bradshaw, P., Dean, R.B., and McEligot, D.M. 1973. Calculation of interacting turbulent shear layers: duct flow. J. Fluids Engg., 95:214-220.

17. Emery, A.F. and Gessner, F.B. 1976. The numerical prediction of the turbulent velocities and temperatures in the developing flow between parallel plates. J. Heat Trans., 98:594-600.

18. Catherall, D. and Mangler, K.W. 1966. The integration of the two-dimensional laminar boundary-layer equations past the point of vanishing skin friction. J. Fluid Mech., 26:163-182.

19. Klineberg, J.M. and Steger, J.L. 1974. On laminar boundary-layer separation. AIAA Paper No. 74-94.

20. Horton, H.P. 1974. Separating laminar boundary layers with prescribed wall shear. AIAA J., 12:1772-1774.

21. Carter, J.E. 1974. Solutions for laminar boundary layers with separation and reattachment. AIAA Paper No. 74-583.

22. Carter, J.E. 1975. Inverse solutions for laminar boundary-layer flows with separation and reattachment. NASA TR R-447.

23. Carter, J.E. and Wornom, S.F. 1975. A forward marching procedure for separated boundary-layer flows. AIAA J., 13:1101-1103.

24. Williams, P.G. 1975. A reverse flow computation in the theory of self-induced separation. Proceedings of the Fourth International Conf. on Numerical Methods in Fluid Dynamics. Vol. 35 of Lecture Notes in Physics, Richtmyer, R.D. (ed.), Springer-Verlag, 445-451.

25. Williams, P.G. 1976. Private communication.

26. Briley, W.R. 1971. A numerical study of laminar separation bubbles using the Navier-Stokes equations. J. Fluid Mech., 47:713-736.

27. Coles, D.E. and Hirst, E.A. 1969. Proceedings of Computation of Turbulent Boundary Layers, 1968 AFOSR-IFP-Stanford Conf., II. Theomosciences Div., Stanford University, Stanford.

28. Cebeci, T. and Bradshaw, P. 1977. Momentum Transfer in Boundary Layers. McGraw-Hill-Hemisphere.

29. Crank, J. and Nicholson, P. 1947. A Practical method for numerical evaluation of solutions of partial-differential equations of the heat-conduction type. Proc. Camb. Phil. Soc. 43:50-67.

30. Keller, H.B. 1978. Numerical methods in boundary-layer theory. Ann. Rev. Fluid Mech., 10:417-33.

31. Keller, H.B. 1974. Accurate difference methods for nonlinear two-point boundary-value problems. SIAM J. Num. Anal. 11:305-20.

32. Reyhner, T.A. and Flugge-Lotz, I. 1968. The interaction of a shock wave with a laminar boundary layer. Int. J. Non-Linear Mech., 3:173-199.

33. Langhaar, H.L. 1942. Steady flow in the transition length of a straight tube. J. Appl. Mech., 9:A-55-58.

34. Campbell, W.D. and Slattery, J.C. 1963. Flow in the entrance of a tube. J. Basic Engg., 41:41-45.

35. Pfenninger, W. 1952. Experiments with laminar flow in the inlet length of a tube at high Reynolds number with and without boundary-layer suction. Northrop Corp., Norair Div. Report.

36. Shapiro, A.H., Siegel, R., and Kline, S.J. 1954. Friction factor in the laminar entry region of a round tube. Proc. 2nd National Congress of Applied Mechanics, ASME, 733-741.

37. Whitelaw, J.H. 1963. Discussion to paper of Campbell and Slattery. J. Basic Engg., 85:45.

38. Schiller, L. 1922. Die Entwichklung der laminaren Geschwindigkeitvetielung und ihre Bedentung fur Zahizkeitmessinger. ZAMM, 2:96-106.

39. Rieman, W. 1928. The value of the Hagenback factor in the determination of viscosity by the efflux method. J. Am. Chem. Soc., 50:46-55.

40. Swindells, J.F., Loe, J.R., and Godfrey, T.B. 1952. J. of Research of N.B.S., 48:1.

41. Siegel, R. and Sparrow, E.M. 1959. Simultaneous development of velocity and temperature distributions in a plot duct with uniform wall heating. AIChE J., 5:73-75.

42. Naito, E. 1975. Laminar heat transfer in the entrance region between parallel plates — the case of uniform heat flux heat transfer. Japanese Res., 4:63-74.

43. Bhatti, M.S. and Savery, C.W. 1977. Heat transfer in the entrance region of a straight channel: laminar flow with uniform wall heat flux. J. Heat Trans., 99:142-144.

44. Bradshaw, P. (ed.) 1976. Topics in Applied Physics, Vol. 12 — Turbulence. Springer, Heidelberg.

45. Barbin, A.R. and Jones, J.B. 1963. Turbulent flow in the inlet region of a smooth pipe. J. Basic Engg., 85:29-34.

46. Laufer, J. 1954. The structure of turbulence in fully developed pipe flows. NACA Rep. 1174.

47. Laufer, J. 1951. Investigation of turbulent flow in a two-dimensional channel. NACA Rep. 1053.

48. Comte-Bellot, G. 1963. Turbulent flow between parallel walls. Ph.D. Thesis, Univ. of Grenoble, France. (Also available as ARC 31 609.)

49. Hussain, A.K.M.F. and Reynolds, W.C. 1975. Measurements in fully developed turbulent channel flow. J. Fluid Engg., 97:568-578.

50. Clark, A.J. 1968. A study of incompressible turbulent boundary layers in channel flow. J. Basic Engg., 90:455.

51. Byrne, J., Hatton, A.P., and Marriott, P.G. 1970. Turbulent flow and heat transfer in the entrance region of a parallel wall passage. Proc. Inst. Mech. Engg., 184:697-710.

52. Dean, R.B. 1976. Interaction of turbulent shear layers in duct flow. Ph.D. Thesis, London University.

53. Stephenson, P.L. 1976. A theoretical study of heat transfer in two-dimensional turbulent flow in a circular pipe and between parallel and diverting plates. Int. J. Heat Mass Transfer, 19:413-423.

54. Hall, W.B. and Khan, S.A. 1964. Experimental investigation into the effect of the thermal boundary condition on heat transfer in the entrance region of a pipe. J. Mech. Engg. Sci., 6:250-255.